

1-1990

Trellis-coded multidimensional phase modulation

S. S. PIETROBON

Robert H. DENG

Singapore Management University, robertdeng@smu.edu.sg

DOI: <https://doi.org/10.1109/18.50375>

Follow this and additional works at: https://ink.library.smu.edu.sg/sis_research



Part of the [Information Security Commons](#)

Citation

PIETROBON, S. S. and DENG, Robert H.. Trellis-coded multidimensional phase modulation. (1990). *IEEE Transactions on Information Theory*. 36, (1), 63-89. Research Collection School Of Information Systems.

Available at: https://ink.library.smu.edu.sg/sis_research/95

This Journal Article is brought to you for free and open access by the School of Information Systems at Institutional Knowledge at Singapore Management University. It has been accepted for inclusion in Research Collection School Of Information Systems by an authorized administrator of Institutional Knowledge at Singapore Management University. For more information, please email libIR@smu.edu.sg.

Trellis-Coded Multidimensional Phase Modulation

STEVEN S. PIETROBON, STUDENT MEMBER, IEEE, ROBERT H. DENG, MEMBER, IEEE,
ALAIN LAFANECHÈRE, GOTTFRIED UNGERBOECK, FELLOW, IEEE, AND
DANIEL J. COSTELLO, JR., FELLOW, IEEE

Abstract—A $2L$ -dimensional multiple phase-shift keyed MPSK ($L \times$ MPSK) signal set is obtained by forming the Cartesian product of L two-dimensional MPSK signal sets. A systematic approach to partitioning $L \times$ MPSK signal sets is used that is based on block coding. An encoder system approach is developed which incorporates the design of a differential precoder, a systematic convolutional encoder, and a signal set mapper. Trellis-coded $L \times 4$ PSK, $L \times 8$ PSK, and $L \times 16$ PSK modulation schemes are found for $1 \leq L \leq 4$ and a variety of code rates and decoder complexities, many of which are fully transparent to discrete phase rotations of the signal set. The new codes achieve asymptotic coding gains up to 5.85 dB.

I. INTRODUCTION

SINCE the publication of the paper by Ungerboeck [1], trellis-coded modulation (TCM) has become a very active research area [2]–[13]. The basic idea of TCM is that by trellis coding onto an expanded signal set (relative to that needed for uncoded transmission), both power and bandwidth efficient communication can be achieved.

TCM can be classified into two basic types, the lattice type (e.g., M -pulse-amplitude modulation (PAM) and M -quadrature amplitude shift keying (QASK)) and the constant amplitude type (e.g., multiple phase-shift keying (MPSK)). Constant amplitude modulation schemes have a lower power efficiency compared with lattice type modulation schemes but are more suitable for certain channels, e.g., satellite channels containing nonlinear amplifiers such as traveling wave tubes (TWT). Taylor and Chan [5] and

Wilson *et al.* [6] have studied the performance of trellis-coded MPSK (TC-MPSK) modulation, in particular rate $2/3$ TC-8PSK and rate $3/4$ TC-16PSK, respectively, for various channel bandwidths and TWT operating points. Their results showed that TC-MPSK modulation schemes are quite robust under typical channel conditions.

In any TCM design, partitioning of the signal set into subsets with increasing minimum intrasubset distances plays a central role. It defines the signal mapping used by the modulator and provides a tight bound on the minimum free Euclidean distance (d_{free}) between code sequences. For lattice-type TCM, Calderbank and Sloane [10] have made the important observation that partitioning the signal set into subsets corresponds to partitioning a lattice into a sublattice and its cosets. Forney [13] has developed a method, called the squaring construction, of constructing higher dimensional lattices from partitioned lower dimensional lattices.

We shall investigate a class of trellis-coded multidimensional (multi-D) MPSK modulation schemes. Signals from a $2L$ -dimensional ($2L$ -D) MPSK signal set (which we shall denote as $L \times$ MPSK) are transmitted over a two-dimensional (2 -D) modulation channel by sending L consecutive signals of an MPSK signal set. Therefore, the $L \times$ MPSK signal set is the Cartesian product of L 2 -D MPSK signal sets. Trellis-coded multi-D phase modulation (TC- $L \times$ MPSK) provides us with a number of advantages that usually cannot be found with TC-MPSK: 1) flexibility in achieving a variety of fractional information rates, 2) codes which are partially or totally transparent to discrete phase rotations of the signal set, 3) suitability for use as inner codes in a concatenated coding system [14], due to their byte oriented nature, and 4) higher decoder speeds resulting from the high rate codes used (rate $k/(k+1)$ with k up to 15 for some codes).

In Section II, we introduce a block coding technique for partitioning $L \times$ MPSK signal sets. Section III contains a description of how the encoder system—comprising a differential precoder, a systematic convolutional encoder, and a multi-D signal set mapper—is obtained for the best codes found in a systematic code search. The signal sets are designed such that the codes can become transparent to integer multiples of $360^\circ/M$ rotations of the MPSK signal set. Also, due to the way in which they are mathe-

Manuscript received January 26, 1987; revised May 18, 1989. This work was supported in part by the National Aeronautics and Space Administration under Grant NAG5-557 and in part by OTC (Australia) R&D Program 4. The material in this paper was partially presented at the IEEE International Symposium on Information Theory, Kobe, Japan, June 1988.

S. S. Pietrobon is with the Department of Electrical and Computer Engineering, University of Notre Dame, Notre Dame, IN 46556 and the School of Electronic Engineering, South Australia Institute of Technology, The Levels, P.O. Box 1, Ingle Farm S.A. 5098, Australia.

R. H. Deng was with the Department of Electrical and Computer Engineering, University of Notre Dame, Notre Dame, IN. He is now with the Institute of Systems Science, National University of Singapore, Kent Ride, Singapore 0511.

A. Lafanechère was with the Department of Electrical and Computer Engineering, Illinois Institute of Technology, Chicago, IL. He is now with Schlumberger Industries, 1 Rue Nieuport, 78141 Velizy, France.

G. Ungerboeck is with the IBM Zurich Research Laboratory, Säumerstrasse 4, CH-8803 Rüschlikon, Switzerland.

D. J. Costello, Jr., is with the Department of Electrical and Computer Engineering, University of Notre Dame, Notre Dame, IN 46556.

IEEE Log Number 8933122.

matically constructed, a signal set mapper can be easily implemented by using basic logic gates and L -bit binary adders. The systematic code search is based on maximizing d_{free} (and thus the asymptotic coding gain) as well as minimizing the number of nearest neighbors (N_{free}) for various degrees of phase transparency. TC- $L \times 4$ PSK, TC- $L \times 8$ PSK, and TC- $L \times 16$ PSK codes for $L=1$ to 4 are found. For TC- $L \times 8$ PSK and TC- $L \times 16$ PSK, asymptotic coding gains up to 5.85 dB compared to an uncoded system are obtained. The TC- $L \times 4$ PSK codes exhibit asymptotic coding gains up to 7.8 dB. Among the $L=1$ codes listed are some new codes that have improvements in N_{free} and phase transparency compared to codes found previously [1], [4], [6], [15]. Viterbi decoding of TC- $L \times$ MPSK is also discussed, concentrating on maximum-likelihood decoding of the parallel transitions within a code trellis.

II. MULTI-D SIGNAL SET PARTITIONING

To describe set partitioning, we will start with the familiar partitioning of the 8PSK signal set. This is followed with an example of multi-D signal set partitioning using the 2×8 PSK signal set. Generalizations will be introduced gradually, so that by the end of this section the reader should become thoroughly familiar with the concepts involved.

A. Partitioning the 8PSK Signal Set

In partitioning the 8PSK signal set, or 1×8 PSK, we form a minimum squared subset distance (MSSD) chain of $\delta_0^2 = 0.586$, $\delta_1^2 = 2$, $\delta_2^2 = 4$, and $\delta_3^2 = \infty$ (assuming that the average signal energy is one). Fig. 1 illustrates this partitioning, in which each subset is equally divided into two smaller subsets such that the MSSD in each smaller subset

is maximized. Partitioning continues in this manner until we have eight subsets, each containing a single point, hence $\delta_3^2 = \infty$.

B. Partitioning 2×8 PSK

A 2×8 PSK signal set ($L = 2$) is illustrated in Fig. 2. We use integers y_1 to indicate the first 8PSK point and y_2 for the second 8PSK point, where $y_1, y_2 \in \{0, 1, \dots, 7\}$. Natural mapping is used to map the integer y_j into each complex-valued 8PSK signal, i.e., $y_j \mapsto \exp[\sqrt{-1}y_j\pi/4]$, for $j=1, 2$. We can also represent y_1 and y_2 in binary form as the vector $y_j = [y_j^2, y_j^1, y_j^0]$, with $y_j^i \in \{0, 1\}$, and where $y_j = 4y_j^2 + 2y_j^1 + y_j^0$, for $j=1, 2$. That is, the least significant bit (LSB) of y_j corresponds to the rightmost bit and the most significant bit (MSB) to the leftmost bit. We will use this convention throughout the paper.

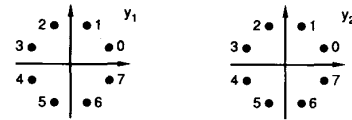


Fig. 2. 2×8 PSK signal set.

To represent a 2×8 PSK signal point, we form the 2×3 binary matrix

$$y = \begin{bmatrix} y_1 \\ y_2 \end{bmatrix} = \begin{bmatrix} y_1^2 & y_1^1 & y_1^0 \\ y_2^2 & y_2^1 & y_2^0 \end{bmatrix}$$

Since a total of 6 bits is used to describe a signal point, the unpartitioned signal set (indicated by Ω^0) has a total of $2^6 = 64$ points. We also say that Ω^0 is at partition level $p = 0$. It can easily be seen that the MSSD at partition

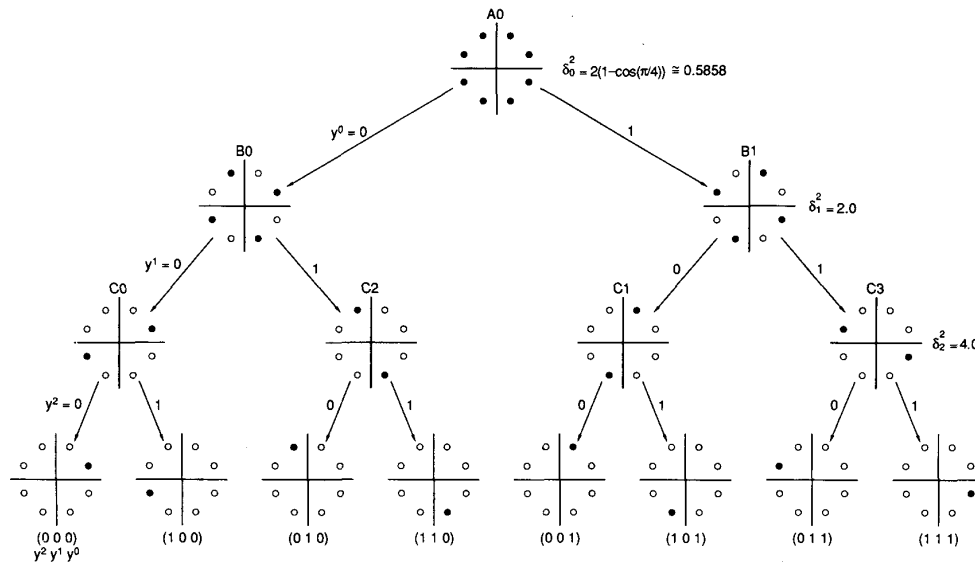


Fig. 1. Signal set partitioning of 8PSK with natural mapping.

level $p = 0$ is $\Delta_0^2 = \delta_0^2 = 0.586$ (we use capital Δ to indicate the MSSD's for $L > 1$ and lower case δ for $L = 1$). The next partition (at partition level $p = 1$) divides Ω^0 into two subsets of 32 points each. We call Ω^1 the subset that contains the all-zero element (i.e., $y_1 = y_2 = 0$). The other subset of 32 points is its coset, labeled $\Omega^1(1)$. In forming these two subsets, we would like their MSSD, Δ_1^2 , to be larger than Δ_0^2 . If this were not possible, then we should find a partitioning that leads to a maximum reduction in the number of nearest neighbors within the smaller subsets (i.e., the average number of signal points that are distance Δ_1^2 away from any point). In principle, the partitioning could be carried out in this heuristic manner.

A more efficient way of partitioning Ω^0 is to require the column vectors of y , i.e., $y^i = [y_1^i, y_2^i]^T$, for $0 \leq i \leq 2$, to be codewords in a block code. This representation using block codes is also known as multilevel coding (first described by Imai and Hirakawa [16] and later applied to quadrature amplitude modulation (QAM) by Cusack [17]). To express this mathematically, we need to introduce some further notation. We define C_{m_i} as that block code which contains the column vectors y^i , for $0 \leq i \leq 2$. Thus C_{m_0} contains the least significant bits of y_1 and y_2 , C_{m_1} contains the middle bits of y_1 and y_2 , and so on. The actual value of m_i indicates which block code is being used. For $L = 2$ only three block codes are of interest to us: C_0 , which is the (2,2) block code with Hamming distance $d_0 = 1$ (and codewords $[0\ 0]^T$, $[0\ 1]^T$, $[1\ 1]^T$, and $[1\ 0]^T$); C_1 , which is the (2,1) block code with Hamming distance $d_1 = 2$ (and codewords $[0\ 0]^T$ and $[1\ 1]^T$); and C_2 , which is the (2,0) block code having only one codeword, $[0\ 0]^T$ and Hamming distance $d_2 = \infty$.

Also, since C_{m_i} denotes a block code with 2^{L-m_i} codewords, we can write that the partition level p is the sum of all the m_i that produce the subset Ω^p , i.e., $p = \sum_{i=0}^2 m_i$. Since there are $I = \log_2 M$ bits needed for each MPSK point, p can range from 0 to IL (0 to 6 in this case). A shorthand way of writing which column vectors y^i belong to which block codes is $\Omega(C_{m_2}, C_{m_1}, C_{m_0})$. Thus we can write $\Omega^0 = \Omega(C_0, C_0, C_0)$. Since C_0 contains all possible length 2 binary vectors, then Ω^0 is generated.

To obtain the next partition (at level $p = 1$), we let $\Omega^1 = \Omega(C_0, C_0, C_1)$. This partition satisfies our previous comments on partitioning. That is, C_1 has only two codewords (reducing the number of points to 32), and C_1 contains the all-zero codeword. In partitioning, we also require the property that all the points in Ω^1 belong to Ω^0 (written as $\Omega^1 \subset \Omega^0$). For this example, since $C_1 \subset C_0$, this property is satisfied. This can be stated more generally as $\Omega^{p+1} \subset \Omega^p$, for $0 \leq p \leq IL - 1$. Thus, if we have two partition levels p and p' , and $p' = p + 1$, then $C_{m'_i} \subseteq C_{m_i}$ for $0 \leq i \leq I - 1$.

The partition Ω^1 is equivalent to forcing the LSB's of both y_1 and y_2 to be either zero or one. By inspection of Fig. 2 we can thus see that $\Delta_1^2 = 2\delta_0^2 = 1.172$. In fact, we can use a more general expression that gives a lower bound on the MSSD. From [18], [19] we have

$$\Delta_p^2 \geq \min(\delta_{I-1}^2 d_{m_{I-1}}, \dots, \delta_1^2 d_{m_1}, \delta_0^2 d_{m_0}) \quad (1)$$

where d_{m_i} is the Hamming distance of the code C_{m_i} , for $0 \leq i \leq I - 1$. From (1), we obtain for 2×8 PSK,

$$\Delta_p^2 \geq \min(4d_{m_2}, 2d_{m_1}, 0.586d_{m_0}). \quad (2)$$

For $p = 0$ and 1, we can see that (2) is satisfied with equality. In fact, due to the symmetry of the 8PSK signal set, (2) is an equality for all values of p . It can be seen that in partitioning Ω^0 into Ω^1 and its coset $\Omega^1(1)$, we could have formed $\Omega(C_0, C_1, C_0)$ or $\Omega(C_1, C_0, C_0)$ instead of $\Omega(C_0, C_0, C_1)$. However, both these other partitions have $\Delta_1^2 = 0.586$ and are therefore not good partitions, since we want Δ_1^2 to be as large as possible. This is because d_{free}^2 can be lower-bounded by $2\Delta_1^2$ for many trellis codes [1].

Ignoring for the moment how the cosets are formed, we can partition Ω^1 into Ω^2 and its coset $\Omega^2(2)$, and so on. (The value within the brackets of the coset will be explained in Section II-C.) Every time we partition, we want to make Δ_p^2 as large as possible. To do this we use the following rule. The C_{m_i} that we partition (into $C_{m_{i+1}}$) from level p to level $p + 1$ should be the i corresponding to the smallest $\delta_i^2 d_{m_i}$ at partition level p . If there are two or more $\delta_i^2 d_{m_i}$ that have the smallest value, we choose the one with the smallest i .

Note that once C_{m_i} has been partitioned to C_2 (or C_{I-1} in general), then that particular block code cannot be further partitioned (since it contains only one codeword). Table I illustrates the partitioning of the 2×8 PSK signal set. The arrows show which C_{m_i} are being partitioned as p is increased. The values of Δ_p^2 are also shown. Note that at $p = 3$, we have $\delta_i^2 d_{m_i} = 4$ for both $i = 1$ and 2. As indicated by the above rule, $i = 1$ is chosen to be partitioned to form Ω^4 . Even though $\Delta_4^2 = \Delta_3^2 = 4$, partition level 4 is still useful for coding since the number of nearest neighbors for Ω^4 is less than for Ω^3 . This will become more apparent when the actual codes are found.

TABLE I
2 × 8PSK SIGNAL SET PARTITION

Partition Level (p)	Ω^p	Minimum Squared Subset Distance (Δ_p^2)	Generator (t^p) ^T
0	$\Omega(C_0, C_0, C_0)$	$\min(4, 2, 0.586) = 0.586$	[0 1]
1	$\Omega(C_0, C_0, C_1)$	$\min(4, 2, 1.172) = 1.172$	[1 1]
2	$\Omega(C_0, C_0, C_2)$	$\min(4, 2, \infty) = 2.0$	[0 2]
3	$\Omega(C_0, C_1, C_2)$	$\min(4, 4, \infty) = 4.0$	[2 2]
4	$\Omega(C_1, C_2, C_2)$	$\min(4, \infty, \infty) = 4.0$	[0 4]
5	$\Omega(C_1, C_2, C_2)$	$\min(8, \infty, \infty) = 8.0$	[4 4]
6	$\Omega(C_2, C_2, C_2)$	$\min(\infty, \infty, \infty) = \infty$	—

The previous rule usually works quite well. For $L = 3$, though, some of the best partitions do not follow this rule. Instead, we can allow a Δ_p^2 to be smaller than the rule proposes, to obtain a larger $\Delta_{p'}^2$ for some $p' > p$ than is possible by following the rule.

C. Formation of Cosets

Now consider partition level $p = 1$. We have shown that there are two subsets, namely Ω^1 and its coset $\Omega^1(1)$. To obtain $\Omega^1(1)$, we must look at how coset codes are derived

from block codes. Recall that C_1 is the (2,1) block code with Hamming distance $d_1=2$. The coset $C_1(1)$ of this code is formed by adding modulo-2 a nonzero codeword that belongs to C_0 but does not belong to C_1 (called the generator τ^0) to all the codewords in C_1 . We illustrate this with an example. C_0 has codewords $[0\ 0]^T$, $[0\ 1]^T$, $[1\ 0]^T$, and $[1\ 1]^T$ (remember that these codewords correspond to column vectors of y), and C_1 has codewords $[0\ 0]^T$ and $[1\ 1]^T$. Therefore, the generator τ^0 could equal $[0\ 1]^T$ or $[1\ 0]^T$. We arbitrarily choose $\tau^0 = [0\ 1]^T$. Thus $C_1(1) = C_1 \oplus \tau^0 = \{[0\ 1]^T, [1\ 0]^T\}$. (In this paper the symbol \oplus will be used to denote modulo-2 (EXCLUSIVE-OR) arithmetic and $+$ to denote integer or modulo- M arithmetic, $M > 2$.) Note that if $\tau^0 = [1\ 0]^T$, the same coset vectors would have been found, except that they would have been in a different order. Also note that the Hamming distance between codewords in $C_1(1)$ is equal to d_1 .

We can also write a general expression for the cosets at partition level $p=1$ as

$$C_1(\zeta^0) = C_1 \oplus \zeta^0 \tau^0 \quad (3)$$

where $\zeta^0 \in \{0,1\}$. Thus when $\zeta^0=0$, we obtain $C_1(0) \equiv C_1$, and when $\zeta^0=1$, we obtain the coset of C_1 , $C_1(1)$. In a similar way we can divide C_1 into C_2 and its coset $C_2(2)$ and $C_1(1)$ into cosets $C_2(1)$ and $C_2(3)$. Fig. 3 gives an illustration of this partition. For the second generator, we have only one choice, i.e., $\tau^1 = [1\ 1]^T$. The general expres-

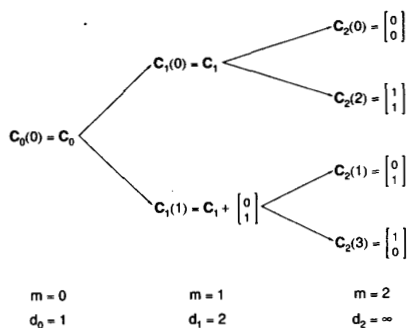


Fig. 3. Partitioning of $L=2$ binary vector space.

sion for the cosets at partition level $p=2$ becomes

$$\begin{aligned} C_2(2\zeta^1 + \zeta^0) &= C_2 \oplus \zeta^1 \tau^1 \oplus \zeta^0 \tau^0 \\ &= \zeta^1 \begin{bmatrix} 1 \\ 1 \end{bmatrix} \oplus \zeta^0 \begin{bmatrix} 0 \\ 1 \end{bmatrix}, \end{aligned} \quad (4)$$

where C_2 is the all-zero vector and $\zeta^m \in \{0,1\}$ for $0 \leq m \leq 1$. We also note that $C_2 \subset C_1 \subset C_0$ and that $\tau^m \in C_m$, but that $\tau^m \notin C_{m+1}$, for $0 \leq m \leq 1$.

Since we have shown how the cosets of C_m are formed, we can now show how the cosets of Ω^p are formed. We start with the simplest case, the single coset of Ω^1 , namely, $\Omega^1(1)$. In the same way as the block codes are partitioned, we must find a 2×3 matrix that belongs to Ω^0 but does not belong to Ω^1 . This is called the *generator* of Ω^1 and is labeled t^0 . Since C_{m_0} is partitioned in going from Ω^0 to Ω^1 , this implies that $t^0 = [\mathbf{0}, \mathbf{0}, \tau^0]$, where $\mathbf{0}$ is the all-zero

vector $[0\ 0]^T$, i.e.,

$$t^0 = \begin{bmatrix} 0 & 0 & 0 \\ 0 & 0 & 1 \end{bmatrix}.$$

An alternate notation for t^0 (using the symbol t^0), is to treat t^0 as if it represented two integer values y_1 and y_2 . Thus t^0 in integer form is $t^0 = [0\ 1]^T$.

To form the coset $\Omega^1(1)$, all that is required is to add t^0 modulo-2 to all the signal points in Ω^1 . We write this as

$$\Omega^1(z^0) = \Omega^1 \oplus z^0 t^0, \quad (5)$$

where $z^0 \in \{0,1\}$ indicates which of the two subsets is being selected. We can see that in coset $\Omega^1(1)$, the LSB's of y_1 and y_2 are either 0 and 1 or 1 and 0, respectively. Thus this coset has the same MSSD as Ω^1 , i.e., $\Delta_1^2 = 1.172$. Alternately, t^0 can be added modulo- M (modulo-8 in this case) to the signal points in Ω^1 . With modulo-8 arithmetic, the LSB's of y_1 and y_2 are still added modulo-2, but the LSB's now produce carries which affect the middle and most significant bits. This is denoted as

$$\Omega^1(z^0) = \Omega^1 + z^0 t^0 \pmod{8}. \quad (6)$$

For example, a signal $y = [1\ 3]^T$ (where $y = [y_1\ y_2]^T$) in Ω^1 becomes $[1\ 2]^T$ with modulo-2 addition of t^0 to y or $[1\ 4]^T$ with modulo-8 addition of t^0 to y . Using either type of arithmetic, we still obtain the required partition, although the ordering of signal points within each coset is different. In constructing rotationally invariant trellis codes, we will find that there is a distinct advantage to using modulo- M arithmetic over modulo-2 arithmetic.

Continuing with the set partitioning, it should be obvious that the next generator is $t^1 = [1\ 1]^T$. From Table I, we see that t^1 corresponds to the generator of C_1 . The expression for the cosets of Ω^2 is

$$\Omega^2(2z^1 + z^0) = \Omega^2 + z^1 \begin{bmatrix} 1 \\ 1 \end{bmatrix} + z^0 \begin{bmatrix} 0 \\ 1 \end{bmatrix} \pmod{8}, \quad (7)$$

where $z^i \in \{0,1\}$, for $0 \leq i \leq 1$. For partition level $p=3$, we choose $t^2 = [0\ 2]^T$, with $z^2 \in \{0,1\}$ used to select t^2 . Continuing in the same way, we can partition the signal set until we obtain only a single (4-D) signal point. Thus we can form the equation (using the generators from Table I)

$$\begin{aligned} y(z) &= \begin{bmatrix} y_1 \\ y_2 \end{bmatrix} = \Omega^6(z) \\ &= z^5 \begin{bmatrix} 4 \\ 4 \end{bmatrix} + z^4 \begin{bmatrix} 0 \\ 4 \end{bmatrix} + z^3 \begin{bmatrix} 2 \\ 2 \end{bmatrix} + z^2 \begin{bmatrix} 0 \\ 2 \end{bmatrix} \\ &\quad + z^1 \begin{bmatrix} 1 \\ 1 \end{bmatrix} + z^0 \begin{bmatrix} 0 \\ 1 \end{bmatrix} \pmod{8} \end{aligned} \quad (8)$$

where $z = \sum_{i=0}^5 2^i z^i$, with $z^i \in \{0,1\}$, for $0 \leq i \leq 5$, and $y(z)$ gives the integer representations of the two 8PSK signal points. The signal set mapping given by z can now be directly used by a convolutional encoder. Since y_1 and y_2 can be described in terms of z , the signal set mapper can be implemented using simple logic circuits (EXCLUSIVE-OR circuits for modulo-2 addition and binary adders for modulo- M addition). Alternatively, since z can be represented with only six bits, one can use a small ROM. Fig. 4

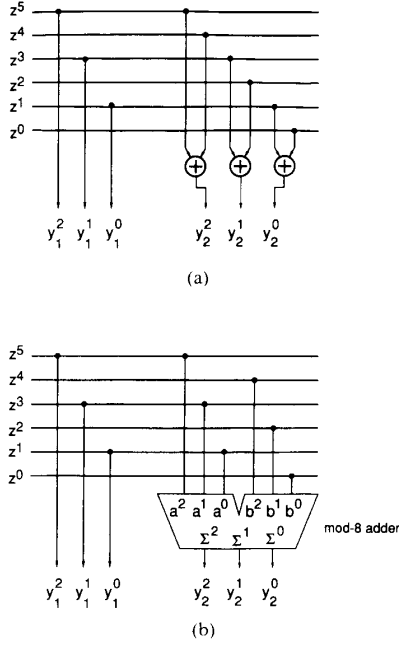


Fig. 4. 2×8 PSK signal set mappers. (a) With modulo-2 addition. (b) with modulo-8 addition.

illustrates two possible signal set mappers for 2×8 PSK. Fig. 4(a) shows a mapper using modulo-2 arithmetic, and Fig. 4(b) shows a mapper using modulo-8 arithmetic.

In general, we can write (8) as

$$y(z) = \begin{bmatrix} y_1 \\ \vdots \\ y_L \end{bmatrix} = \Omega^{IL}(z) = \sum_{i=0}^{IL-1} z^i t^i \quad (9)$$

where $z = \sum_{i=0}^{IL-1} 2^i z^i$, with $z^i \in \{0, 1\}$, for $0 \leq i \leq IL - 1$.

The addition in (9) is not specified but may be modulo-2 (using the binary matrix generators), modulo- M (using the integer generators), or a combination of modulo-2 and modulo- M . Fig. 5 illustrates the partitioning of Ω^0 into Ω^3 and its cosets $\Omega^3(4z^2 + 2z^1 + z^0)$ for the 2×8 PSK signal set using modulo-8 addition.

D. Partitioning $3 \times$ MPSK and $4 \times$ MPSK Signal Sets

In a similar fashion to 2×8 PSK, to partition $L \times 8$ PSK (for $L > 2$) requires the partitioning of length $L > 2$ block codes. We again look for partitions that have an increasing Hamming distance. For $L = 3$, there are two partitions that are interesting.

The first partition has Hamming distances $d_0 = 1$, $d_1^1 = 2$, $d_2^1 = 2$, and $d_3 = \infty$. These Hamming distances correspond to the (3,3), (3,2), (3,1), and (3,0) block codes C_0 , C_1^1 , C_2^1 , and C_3 , respectively, where $C_3 \subset C_2^1 \subset C_1^1 \subset C_0$. Table II-a)

TABLE II
BINARY GENERATORS FOR $L = 3$ AND 4

a) $L = 3$ (I)			
m	d_m	N_m	$(\tau_1^m)^T$
0	1	3	[1 1 1]
1	2	3	[1 1 0]
2	2	1	[0 1 1]
b) $L = 3$ (II)			
m	d_m	N_m	$(\tau_2^m)^T$
0	1	3	[0 0 1]
1	1	1	[0 1 1]
2	3	1	[1 1 1]
c) $L = 4$			
m	d_m	N_m	$(\tau^m)^T$
0	1	4	[0 0 0 1]
1	2	6	[0 0 1 1]
2	2	2	[0 1 0 1]
3	4	1	[1 1 1 1]

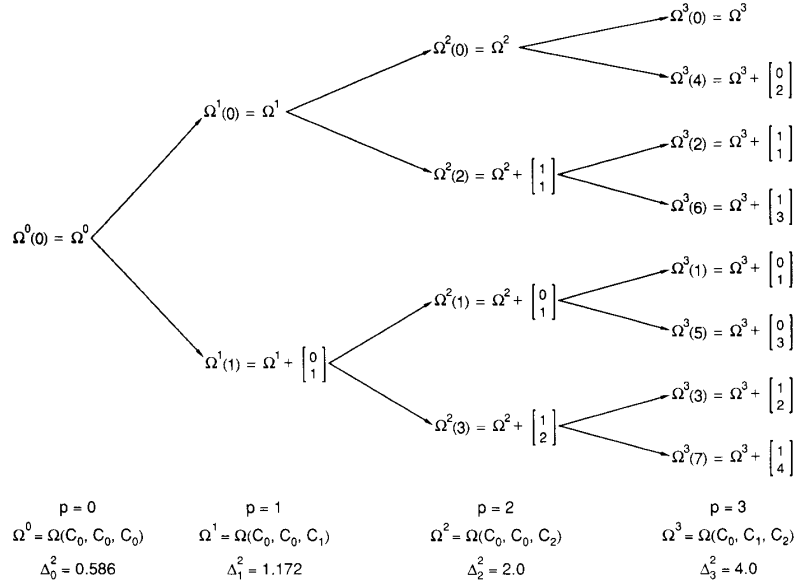


Fig. 5. Three-level 2×8 PSK signal set partition.

gives the three generators, τ_1^0 , τ_1^1 , and τ_1^2 , that were chosen, along with the Hamming distances (d_m) and the number of nearest neighbors (N_m) at each partition level m . The choice was not completely arbitrary, since one of the generators must be the all-ones vector (which in this case is τ_1^0). The reason for this will be explained in Section III.

It is interesting to note that the generator matrix for these block codes can be formed from the generators. In general, a generator matrix G_m for an $(L, L-m)$ block code C_m , for $0 \leq m \leq L-1$, can be formed from the generators τ^m to τ^{L-1} , i.e., $G_m = [\tau^m, \tau^{m+1}, \dots, \tau^{L-1}]^T$. For example, for the $L=3$ block codes given in Table II-a),

$$G_0^1 = \begin{bmatrix} 1 & 1 & 1 \\ 1 & 1 & 0 \\ 0 & 1 & 1 \end{bmatrix} \quad G_1^1 = \begin{bmatrix} 1 & 1 & 0 \\ 0 & 1 & 1 \end{bmatrix}$$

$$G_2^1 = [0 \quad 1 \quad 1].$$

For the other $L=3$ partition, we have $d_0=1$, $d_1^2=1$, $d_2^2=3$, and $d_3=\infty$. These distances correspond to block codes C_0 , C_1^2 , C_2^2 , and C_3 , where $C_3 \subset C_2^2 \subset C_1^2 \subset C_0$. Table II-b) shows the generators for these codes. Note that τ_2^2 is the all-ones vector in this case. The advantage of this partition is that $d_2^2=3$ is larger than $d_1^2=2$. However, $d_1^2=1$ is less than $d_1^1=2$.

The partitions of 3×8 PSK that will be useful for trellis coding are given in Tables III-V. Table III corresponds to

TABLE III
3 × 8PSK SIGNAL SET PARTITION (I)

Partition Level (p)	Ω^p	Minimum Squared Subset Distance (Δ_p^2)	Generator $(t^p)^T$
0	$\Omega(C_0, C_0, C_0)$	$\min(4, 2, 0.586) = 0.586$	[1 1 1]
1	$\Omega(C_0, C_0, C_1^1)$	$\min(4, 2, 1.172) = 1.172$	[1 1 0]
2	$\Omega(C_0, C_0, C_2^1)$	$\min(4, 2, 1.172) = 1.172$	[0 1 1]
3	$\Omega(C_0, C_0, C_3)$	$\min(4, 2, \infty) = 2.0$	[2 2 2]
4	$\Omega(C_0, C_1^1, C_3)$	$\min(4, 4, \infty) = 4.0$	[2 2 0]
5	$\Omega(C_0, C_2^1, C_3)$	$\min(4, 4, \infty) = 4.0$	[0 2 2]
6	$\Omega(C_0, C_3, C_3)$	$\min(4, \infty, \infty) = 4.0$	[4 4 4]
7	$\Omega(C_1^1, C_3, C_3)$	$\min(8, \infty, \infty) = 8.0$	[4 4 0]
8	$\Omega(C_2^1, C_3, C_3)$	$\min(8, \infty, \infty) = 8.0$	[0 4 4]
9	$\Omega(C_3, C_3, C_3)$	$\min(\infty, \infty, \infty) = \infty$	—

TABLE IV
3 × 8PSK SIGNAL SET PARTITION (II)

Partition Level (p)	Ω^p	Minimum Squared Subset Distance (Δ_p^2)	Generator $(t^p)^T$
0	$\Omega(C_0, C_0, C_0)$	$\min(4, 2, 0.586) = 0.586$	[0 0 1]
1	$\Omega(C_0, C_0, C_1^2)$	$\min(4, 2, 0.586) = 0.586$	[0 1 1]
2	$\Omega(C_0, C_0, C_2^2)$	$\min(4, 2, 1.757) = 1.757$	[1 1 1]
3	$\Omega(C_0, C_0, C_3)$	$\min(4, 2, \infty) = 2.0$	[2 2 2]
4	$\Omega(C_0, C_1^1, C_3)$	$\min(4, 4, \infty) = 4.0$	[2 2 0]
5	$\Omega(C_0, C_2^1, C_3)$	$\min(4, 4, \infty) = 4.0$	[0 2 2]
6	$\Omega(C_0, C_3, C_3)$	$\min(4, \infty, \infty) = 4.0$	[4 4 4]
7	$\Omega(C_1^1, C_3, C_3)$	$\min(8, \infty, \infty) = 8.0$	[4 4 0]
8	$\Omega(C_2^1, C_3, C_3)$	$\min(8, \infty, \infty) = 8.0$	[0 4 4]
9	$\Omega(C_3, C_3, C_3)$	$\min(\infty, \infty, \infty) = \infty$	—

TABLE V
3 × 8PSK SIGNAL SET PARTITION (III)

Partition Level (p)	Ω^p	Minimum Squared Subset Distance (Δ_p^2)	Generator $(t^p)^T$
0	$\Omega(C_0, C_0, C_0)$	$\min(4, 2, 0.586) = 0.586$	[0 0 1]
1	$\Omega(C_0, C_0, C_1^2)$	$\min(4, 2, 0.586) = 0.586$	[0 1 1]
2	$\Omega(C_0, C_0, C_2^2)$	$\min(4, 2, 1.757) = 1.757$	[1 1 1]
3	$\Omega(C_0, C_0, C_3)$	$\min(4, 2, \infty) = 2.0$	[0 0 2]
4	$\Omega(C_0, C_1^2, C_3)$	$\min(4, 2, \infty) = 2.0$	[0 2 2]
5	$\Omega(C_0, C_2^2, C_3)$	$\min(4, 6, \infty) = 4.0$	[4 4 4]
6	$\Omega(C_1^2, C_3, C_3)$	$\min(8, 6, \infty) = 6.0$	[2 2 2]
7	$\Omega(C_2^2, C_3, C_3)$	$\min(8, \infty, \infty) = 8.0$	[4 4 0]
8	$\Omega(C_3, C_3, C_3)$	$\min(8, \infty, \infty) = 8.0$	[0 4 4]
9	$\Omega(C_3, C_3, C_3)$	$\min(\infty, \infty, \infty) = \infty$	—

the first partition where we try to maximize Δ_p^2 at each partition level. In Tables IV and V, the second set of block codes are used to increase Δ_2^2 to 1.757 while Δ_1^2 decreases to 0.586. In Table V, Δ_6^2 increases to 6.0 and Δ_4^2 decreases to 2.0. Note how $\Delta_6^2 = 6.0$ is obtained in Table V. At $p=4$ we have $\Delta_4^2 = \min(4.0, 2.0, \infty)$ and at the next partition level, $\Delta_5^2 = \min(4.0, 6.0, \infty) = 4.0$. Now C_{m_2} is partitioned to give $\Delta_6^2 = \min(8.0, 6.0, \infty) = 6.0$. In the next level we partition C_{m_1} to obtain $\Delta_7^2 = 8.0$. In Section III the reasons why these latter two partitions are used will be seen more clearly.

For $L=4$ there is only one good way to partition length 4 block codes. Table II-c) gives a summary of the basic parameters. Using Table II-c), we can partition the 4×8 PSK signal set as shown in Table VI.

For $L \times 4$ PSK and $L \times 16$ PSK we obtain from (1) that

$$\Delta_p^2 \geq \min(4d_{m_1}, 2d_{m_0}) \quad (10a)$$

$$\Delta_p^2 \geq \min(4d_{m_3}, 2d_{m_2}, 0.586d_{m_1}, 0.152d_{m_0}), \quad (10b)$$

respectively, where $p = \sum_{i=0}^{I-1} m_i$ ($I=2$ for (10a) and $I=4$ for (10b)). In a similar fashion to $L \times 8$ PSK, the signal set

TABLE VI
4 × 8PSK SIGNAL SET PARTITION

Partition Level (p)	Ω^p	Minimum Squared Subset Distance (Δ_p^2)	Generator $(t^p)^T$
0	$\Omega(C_0, C_0, C_0)$	$\min(4, 2, 0.586) = 0.586$	[0 0 0 1]
1	$\Omega(C_0, C_0, C_1^1)$	$\min(4, 2, 1.172) = 1.172$	[0 0 1 1]
2	$\Omega(C_0, C_0, C_2^1)$	$\min(4, 2, 1.172) = 1.172$	[0 1 0 1]
3	$\Omega(C_0, C_0, C_3)$	$\min(4, 2, 2.343) = 2.0$	[0 0 0 2]
4	$\Omega(C_0, C_1, C_3)$	$\min(4, 4, 2.343) = 2.343$	[1 1 1 1]
5	$\Omega(C_0, C_1, C_4)$	$\min(4, 4, \infty) = 4.0$	[0 0 2 2]
6	$\Omega(C_0, C_2, C_4)$	$\min(4, 4, \infty) = 4.0$	[0 2 0 2]
7	$\Omega(C_0, C_3, C_4)$	$\min(4, 8, \infty) = 4.0$	[0 0 0 4]
8	$\Omega(C_1, C_3, C_4)$	$\min(8, 8, \infty) = 8.0$	[2 2 2 2]
9	$\Omega(C_1, C_4, C_4)$	$\min(8, \infty, \infty) = 8.0$	[0 0 4 4]
10	$\Omega(C_2, C_4, C_4)$	$\min(8, \infty, \infty) = 8.0$	[0 4 0 4]
11	$\Omega(C_3, C_4, C_4)$	$\min(16, \infty, \infty) = 16.0$	[4 4 4 4]
12	$\Omega(C_4, C_4, C_4)$	$\min(\infty, \infty, \infty) = \infty$	—

TABLE VII
SUMMARY OF $L \times 4$ PSK PARTITIONS

Partition Level (p)	$L = 2$		$L = 3$ (I)		$L = 3$ (II)		$L = 3$ (III)		$L = 4$	
	MSSD (Δ_p^2)	Gen. ($(t^p)^T$)	MSSD (Δ_p^2)	Gen. ($(t^p)^T$)	MSSD (Δ_p^2)	Gen. ($(t^p)^T$)	MSSD (Δ_p^2)	Gen. ($(t^p)^T$)	MSSD (Δ_p^2)	Gen. ($(t^p)^T$)
0	2	01	2	111	2	001	2	001	2	0001
1	4	11	4	110	2	011	2	011	4	0011
2	4	02	4	011	4	222	4	002	4	0101
3	8	22	4	222	6	111	4	022	4	0002
4	—	—	8	220	8	220	6	111	8	1111
5	—	—	8	022	8	022	12	222	8	0022
6	—	—	—	—	—	—	—	—	8	0202
7	—	—	—	—	—	—	—	—	16	2222
$p_0 p_1$	1	3	0	3	3	2	4	5	4	7

TABLE VIII
SUMMARY OF $L \times 8$ PSK PARTITIONS

Partition Level (p)	$L = 2$		$L = 3$ (I)		$L = 3$ (II)		$L = 3$ (III)		$L = 4$						
	MSSD (Δ_p^2)	Gen. ($(t^p)^T$)	MSSD (Δ_p^2)	Gen. ($(t^p)^T$)	MSSD (Δ_p^2)	Gen. ($(t^p)^T$)	MSSD (Δ_p^2)	Gen. ($(t^p)^T$)	MSSD (Δ_p^2)	Gen. ($(t^p)^T$)					
0	0.586	01	0.586	111	0.586	001	0.586	001	0.586	0001					
1	1.172	11	1.172	110	0.586	011	0.586	011	1.172	0011					
2	2	02	1.172	011	1.757	111	1.757	111	1.172	0101					
3	4	22	2	222	2	222	2	002	2	0002					
4	4	04	4	220	4	220	2	022	2.343	1111					
5	8	44	4	022	4	022	4	444	4	0022					
6	—	—	4	444	4	444	6	222	4	0202					
7	—	—	8	440	8	440	8	440	4	0004					
8	—	—	8	044	8	044	8	044	8	2222					
9	—	—	—	—	—	—	—	—	8	0044					
10	—	—	—	—	—	—	—	—	8	0404					
11	—	—	—	—	—	—	—	—	16	4444					
$p_0 p_1 p_2$	1	3	5	0	3	6	2	3	6	2	6	5	4	8	11

TABLE IX
SUMMARY OF $L \times 16$ PSK PARTITIONS

Partition Level (p)	$L = 2$		$L = 3$ (I)		$L = 3$ (II)		$L = 3$ (III)		$L = 4$											
	MSSD (Δ_p^2)	Gen. ($(t^p)^T$)	MSSD (Δ_p^2)	Gen. ($(t^p)^T$)	MSSD (Δ_p^2)	Gen. ($(t^p)^T$)	MSSD (Δ_p^2)	Gen. ($(t^p)^T$)	MSSD (Δ_p^2)	Gen. ($(t^p)^T$)										
0	0.152	01	0.152	111	0.152	001	0.152	001	0.152	0001										
1	0.304	11	0.304	110	0.152	011	0.152	011	0.304	0011										
2	0.586	02	0.304	011	0.457	111	0.457	111	0.304	0101										
3	1.172	22	0.586	222	0.586	222	0.586	002	0.586	0002										
4	2	04	1.172	220	1.172	220	0.586	022	0.609	1111										
5	4	44	1.172	022	1.172	022	1.757	222	1.172	0022										
6	4	08	2	444	2	444	2	444	1.172	0202										
7	8	88	4	440	4	440	4	440	2	0004										
8	—	—	4	044	4	044	4	044	2.343	2222										
9	—	—	4	888	4	888	4	888	4	0044										
10	—	—	8	880	8	880	8	880	4	0404										
11	—	—	8	088	8	088	8	088	4	0008										
12	—	—	—	—	—	—	—	—	8	4444										
13	—	—	—	—	—	—	—	—	8	0088										
14	—	—	—	—	—	—	—	—	8	0808										
15	—	—	—	—	—	—	—	—	16	8888										
$p_0 p_1 p_2 p_3$	1	3	5	7	0	3	6	9	2	3	6	9	2	5	6	9	4	8	12	15

partitions can be obtained for $L = 2$ to 4. Tables VII, VIII, IX give a summary of the partitions for $L \times 4$ PSK, $L \times 8$ PSK, and $L \times 16$ PSK, respectively.

E. Larger Dimensional MPSK Signal Sets and the Squaring Construction

One way to obtain larger dimensional MPSK signal sets is to take an $L \times$ MPSK signal set partition (with its corresponding MSSD's relabeled as δ_i^2 , for $0 \leq i \leq IL$) and

form a $2LL'$ dimensional MPSK signal set which we label as $L' \times L \times$ MPSK. Thus, if we have a 2×8 PSK signal set, the MSSD's Δ_p^2 , $0 \leq p \leq 6L'$, for $L' \times 2 \times 8$ PSK are given by

$$\Delta p^2 \geq \min(8d_{m_5}, 4d_{m_4}, 4d_{m_3}, 2d_{m_2}, 1.172d_{m_1}, 0.586d_{m_0}) \quad (11)$$

where the d_{m_i} are the Hamming distances of $(L', L' - m_i)$ block codes. If $L' = 2$ we can form the $2 \times 2 \times 8$ PSK signal

TABLE X
 $2 \times 2 \times 8$ PSK SIGNAL SET PARTITION

p	Ω^p	Minimum Squared Subset Distance (Δ_p^2)	Gen. (t^p) ^T
0	$\Omega(C_0, C_0, C_0, C_0, C_0, C_0, C_0)$	$\min(8, 4, 4, 2, 1.172, 0.586) = 0.586$	[0 1]
1	$\Omega(C_0, C_0, C_0, C_0, C_0, C_0, C_1)$	$\min(8, 4, 4, 2, 1.172, 1.172) = 1.172$	[1 1]
2	$\Omega(C_0, C_0, C_0, C_0, C_0, C_1, C_2)$	$\min(8, 4, 4, 2, 1.172, \infty) = 1.172$	[0 2]
3	$\Omega(C_0, C_0, C_0, C_1, C_1, C_2)$	$\min(8, 4, 4, 2, 2.343, \infty) = 2.0$	[0 4]
4	$\Omega(C_0, C_0, C_0, C_1, C_1, C_2)$	$\min(8, 4, 4, 4, 2.343, \infty) = 2.343$	[2 2]
5	$\Omega(C_0, C_0, C_0, C_1, C_2, C_2)$	$\min(8, 4, 4, 4, \infty, \infty) = 4.0$	[4 4]
6	$\Omega(C_0, C_0, C_0, C_2, C_2, C_2)$	$\min(8, 4, 4, \infty, \infty, \infty) = 4.0$	[0 8]
7	$\Omega(C_0, C_0, C_1, C_1, C_2, C_2)$	$\min(8, 4, 8, \infty, \infty, \infty) = 4.0$	[0 16]
8	$\Omega(C_0, C_1, C_1, C_2, C_2, C_2)$	$\min(8, 8, 8, \infty, \infty, \infty) = 8.0$	[8 8]
9	$\Omega(C_0, C_1, C_2, C_2, C_2, C_2)$	$\min(8, 8, \infty, \infty, \infty, \infty) = 8.0$	[16 16]
10	$\Omega(C_1, C_2, C_2, C_2, C_2, C_2)$	$\min(8, \infty, \infty, \infty, \infty, \infty) = 8.0$	[0 32]
11	$\Omega(C_1, C_2, C_2, C_2, C_2, C_2)$	$\min(16, \infty, \infty, \infty, \infty, \infty) = 16.0$	[32 32]
12	$\Omega(C_2, C_2, C_2, C_2, C_2, C_2)$	$\min(\infty, \infty, \infty, \infty, \infty, \infty) = \infty$	—

set, which is equivalent to the 4×8 PSK signal set. Table X illustrates this partitioning. Note that the MSSD's obtained are exactly the same as those found with the 4×8 PSK partitioning given in Table VI. Fig. 6 shows a block diagram of a signal set mapper for the partition of $2 \times 2 \times 8$ PSK. The function T_1 corresponds to the mapping given by the generators in Table X and T_2 to the generators in Table I.

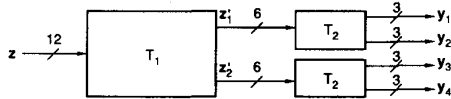


Fig. 6. Block diagram of $2 \times 2 \times 8$ PSK signal set mapper.

For $L' = 2$, the above method of obtaining larger dimensional MPSK is essentially equivalent to the squaring or two-construction described by Forney [13]. The cubing or three-construction corresponds to $L' = 3$. One can continue squaring or cubing various multi-D signal sets in an iterative fashion to obtain many larger dimensional signal sets. If we desire an $L \times$ MPSK signal set, all that is

required is to factor L to determine which constructions are needed. For example, if $L = 24$, we could factor this into a $2 \times 2 \times 2 \times 3 \times 8$ PSK signal set. If L is a prime number, then the appropriate length L block codes and their corresponding generators must be found.

Table XI gives the generators for $L = 5$ and 7. Also given are the Hamming distances and the number of nearest neighbors for each length L block code. Note that there are three different partitions for $L = 5$ and four different partitions for $L = 7$. This suggests that the number of useful partitions increases by one for each successive prime number. Thus $L = 11$ is expected to have five useful partitions, and so on. These partitions were constructed by hand and probably represent the practical limit of hand constructions. For $L = 11$ and above, an algorithmic or mathematical method is required. In forming each partition, we have tried to maximize the Hamming distance and minimize the number of nearest neighbors. For example, the type IV partition maximizes the Hamming distance and minimizes the number of nearest neighbors for the (7, 4) block code while the type III partition maximizes the Hamming distance and minimizes the number of nearest neighbors for the (7, 3) and (7, 2) block codes.

TABLE XI
 BINARY GENERATORS FOR $L = 5$ AND 7

m	$L = 5$ (I)			$L = 5$ (II)			$L = 5$ (III)			d_m	N_m	$(\tau_4^m)^T$
	d_m	N_m	$(\tau_1^m)^T$	d_m	N_m	$(\tau_2^m)^T$	d_m	N_m	$(\tau_3^m)^T$			
0	1	5	[11111]	1	5	[11111]	1	5	[00001]			
1	2	10	[00011]	1	2	[00001]	1	1	[00010]			
2	2	4	[00101]	2	2	[00110]	2	3	[00101]			
3	2	1	[11000]	3	2	[10101]	2	1	[01001]			
4	4	1	[01111]	4	1	[01111]	5	1	[11111]			
			$L = 7$ (I)			$L = 7$ (II)			$L = 7$ (III)		$L = 7$ (IV)	
0	1	7	[1111111]	1	7	[1111111]	1	7	[0000001]	1	7	[0000001]
1	2	21	[0000011]	1	2	[0000001]	1	1	[0001000]	1	3	[0001000]
2	2	9	[0001001]	2	5	[0000101]	2	6	[1111111]	1	1	[1000000]
3	2	3	[0010010]	2	1	[0100010]	2	2	[0000101]	3	7	[0110100]
4	2	1	[0001100]	3	3	[0011100]	3	2	[0101010]	3	3	[0011010]
5	4	2	[1111000]	4	2	[0001111]	4	1	[1100011]	3	1	[0001101]
6	6	1	[0111111]	6	1	[1110111]	5	1	[0011111]	7	1	[1111111]

For larger dimensions, these methods may produce block codes which do not have the largest possible minimum distance. For example, the largest Hamming distance that can be obtained for the (24,12) coset code is six. However, the (24,12) Golay code has a Hamming distance of eight. For $L = 2, 3$, and 4, the block codes are relatively simple. Thus we are fairly certain that the best partitions for these $L \times \text{MPSK}$ signal sets have been found.

III. TRELLIS CODED MULTI-D MPSK DESIGN

This section describes how convolutional codes are constructed for the $L \times \text{MPSK}$ signal sets described previously. We first show how to construct signal sets that have good phase rotation properties. Following this, a method used to find good convolutional codes based on the parity check equations is presented.

A. Construction of Signal Sets

Equation (9) can be used to describe a signal point in an $L \times \text{MPSK}$ signal set. The number of bits z^j needed to describe each signal point is IL . If the LSB is used for coding, we can form a rate $(IL-1)/IL$ code. A more convenient measure of rate is to use the average number of information bits transmitted during each 2-D signal period T . This is called the *effective rate* of the code, $R_{\text{eff}} = (IL-1)/L$ (bit/T). The unit bit/s/Hz can also be used (for the actual bandwidth efficiency), but this assumes that perfect Nyquist filtering is used in the receive and transmit filters. Since this is not the case in many practical systems, we make a distinction between the units bit/T and bit/s/Hz.

Other rates can be achieved by setting the q LSB's of the mapping to zero. We do this to ensure that the MSSD's are as large as possible, so that the best codes can be found. In this case (9) can be rewritten as

$$y^q(z) = \begin{bmatrix} y_1 \\ \vdots \\ y_L \end{bmatrix} = \sum_{j=q}^{IL-1} z^{j-qt} t^j, \quad (12)$$

for $0 \leq z \leq 2^{IL-q-1} - 1$, $0 \leq q \leq L-1$, and where $y^q(z)$ represents a point z in an $L \times \text{MPSK}$ signal set such that the first q bits of (9) are zero. As before, we do not restrict the type of addition that is used. We now let $z = [z^{IL-q-1}, \dots, z^1, z^0]$, where z is the binary representation of z , and the LSB of z is always the coding bit. This notation ensures that the parity check equations of a convolutional code can always be expressed in terms of the LSB's of z without depending on the type of signal set used or its partitioning. From (12), codes with effective rates $R_{\text{eff}} = (IL-q-1)/L$ can be formed. An upper limit of $q = L-1$ is set because for $q \geq L$ the signal set is partitioned such that $d_{m_0} = \infty$, i.e., an $M/2^j$ -PSK, for $j \geq 1$, signal set is being used (one exception is the $4 \times 8\text{PSK}$ signal set (Table VI) where $d_{m_0} = 4$ for $q = L$). The MSSD's range from Δ_q^2 to Δ_L^2 , and the uncoded minimum squared Euclidean distance (MSED) is Δ_{q+1}^2 , since uncoded trans-

mission uses only half as many signals as coded transmission.

Example 3.1: We can form a rate 4/5 code with an effective rate of 2.0 bit/T from a $2 \times 8\text{PSK}$ ($L = 2$, $I = 3$) signal set with $q = 1$. Then

$$y^1(z) = z^4 \begin{bmatrix} 4 \\ 4 \end{bmatrix} + z^3 \begin{bmatrix} 0 \\ 4 \end{bmatrix} + z^2 \begin{bmatrix} 2 \\ 2 \end{bmatrix} + z^1 \begin{bmatrix} 0 \\ 2 \end{bmatrix} + z^0 \begin{bmatrix} 1 \\ 1 \end{bmatrix} \pmod{8}.$$

The uncoded MSED is $\Delta_2^2 = 2.0$, which is the same as uncoded 4PSK.

B. Effect of a $360^\circ/M$ Phase Rotation on a Multi-D MPSK Signal Set

Using modulo- M arithmetic in (12), multi-D signal sets can be constructed such that there are at most I bits in z affected by a signal set rotation of $\Psi \equiv 360^\circ/M$. For 4PSK, 8PSK, and 16PSK, this corresponds to rotations of 90° , 45° , and 22.5° , respectively. Initially, we consider all possible mapped bits, i.e., $q = 0$.

Consider that a $1 \times \text{MPSK}$ signal set has been rotated by Ψ . Since we are using natural mapping, the integer representation of the rotated signal point is $y_r = y + 1 \pmod{M}$, where y is the integer representation of the signal point before rotation. If y is in binary notation, then

$$y_r^0 = y^0 \oplus 1 = \overline{y^0} \quad (13a)$$

$$y_r^1 = y^1 \oplus y^0 \quad (13b)$$

$$y_r^2 = y^2 \oplus y^0 \cdot y^1 \quad (13c)$$

\vdots

If there are $I = \log_2 M$ bits in a signal set, then we see from (13) that all I bits are affected by a phase rotation of Ψ .

Consider the $2 \times 8\text{PSK}$ signal set, with the mapping given by (8). The phase rotation equations of this mapping can be determined as follows. From (8), the signal outputs can be written in terms of z as

$$\begin{bmatrix} y_1 \\ y_2 \end{bmatrix} = (4z^5 + 2z^3 + z^1) \begin{bmatrix} 1 \\ 1 \end{bmatrix} + (4z^4 + 2z^2 + z^0) \begin{bmatrix} 0 \\ 1 \end{bmatrix} \pmod{8}. \quad (14)$$

After a 45° phase rotation, we have $y_{j,r} = y_j + 1 \pmod{8}$, for $j = 1, 2$. From (14), we can form the following phase rotation equations,

$$\begin{bmatrix} y_{1,r} \\ y_{2,r} \end{bmatrix} = (4z^5 + 2z^3 + z^1 + 1) \begin{bmatrix} 1 \\ 1 \end{bmatrix} + (4z^4 + 2z^2 + z^0) \begin{bmatrix} 1 \\ 1 \end{bmatrix} \pmod{8}.$$

Note that a 1 is added to the term whose coset is $[1 \ 1]^T$. Hence this term "absorbs" the effect of the phase rotation, leaving the remaining term unaffected. As can be seen, bits z^5 , z^3 , and z^1 are affected in a manner similar to y^2 , y^1 , and y^0 in (13), and bits z^4 , z^2 , and z^0 are unaffected by

the phase rotation. Thus we can form the phase rotation equations

$$\begin{aligned} z_r^0 &= z^0 & z_r^2 &= z^2 & z_r^4 &= z^4 \\ z_r^1 &= z^1 \oplus 1 & z_r^3 &= z^3 \oplus z^1 & z_r^5 &= z^5 \oplus z^1 \cdot z^3. \end{aligned} \quad (15)$$

If the signal set had been constructed using modulo-2 addition (instead of modulo-8), only z^0 would have remained unchanged by a 45° phase rotation.

Using general notation, we can express (14) as

$$\begin{bmatrix} y_1 \\ \vdots \\ y_L \end{bmatrix} = (2^{l-1}z^{p_{l-1}} + \dots + 2z^{p_1} + z^{p_0}) \begin{bmatrix} 1 \\ \vdots \\ 1 \end{bmatrix} + 2^{l-1}\{g_{l-1}\} + \dots + 2\{g_1\} + \{g_0\} \pmod{M}, \quad (16)$$

where p_j , for $0 \leq j \leq l-1$, corresponds to those partition levels where t^p equals the vector $[2^j, 2^j, \dots, 2^j]^T$. The term g_j , for $0 \leq j \leq l-1$, corresponds to those remaining terms that have at least one (but not all) component in t^p with value 2^j . For (14) we would have $p_0=1$, $p_1=3$, and $p_2=5$. These values of p_j are given for all the signal set partitions shown in Tables VII-IX. We can now write the phase rotation equations as

$$z_r^{p_0} = z^{p_0} \oplus 1, \quad z_r^{p_1} = z^{p_1} \oplus z^{p_0}, \quad z_r^{p_2} = z^{p_2} \oplus z^{p_0} \cdot z^{p_1}, \dots \quad (17)$$

and for all other partition levels $z^p = z^p$.

For $L=2$, there is only one term in each g_j . However, for $L \geq 3$, there are two or more terms in each g_j . Since the terms in g_j do not contribute to the phase rotational properties of the signal mapping, these terms can be added modulo-2 before being added modulo- M to the other terms. This is best illustrated with an example. For the 3×8 PSK (I) signal set in Table III, we have the following mapping equation:

$$\begin{aligned} \begin{bmatrix} y_1 \\ y_2 \\ y_3 \end{bmatrix} &= z^8 \begin{bmatrix} 0 \\ 4 \\ 4 \end{bmatrix} + z^7 \begin{bmatrix} 4 \\ 4 \\ 0 \end{bmatrix} + z^6 \begin{bmatrix} 4 \\ 4 \\ 4 \end{bmatrix} + z^5 \begin{bmatrix} 0 \\ 2 \\ 2 \end{bmatrix} + z^4 \begin{bmatrix} 2 \\ 2 \\ 0 \end{bmatrix} \\ &\quad + z^3 \begin{bmatrix} 2 \\ 2 \\ 2 \end{bmatrix} + z^2 \begin{bmatrix} 0 \\ 1 \\ 1 \end{bmatrix} + z^1 \begin{bmatrix} 1 \\ 1 \\ 0 \end{bmatrix} + z^0 \begin{bmatrix} 1 \\ 1 \\ 1 \end{bmatrix} \\ &= (4z^6 + 2z^3 + z^0) \begin{bmatrix} 1 \\ 1 \\ 1 \end{bmatrix} + 4 \left\{ z^8 \begin{bmatrix} 0 \\ 1 \\ 1 \end{bmatrix} \oplus z^7 \begin{bmatrix} 1 \\ 1 \\ 0 \end{bmatrix} \right\} \\ &\quad + 2 \left\{ z^5 \begin{bmatrix} 0 \\ 1 \\ 1 \end{bmatrix} \oplus z^4 \begin{bmatrix} 1 \\ 1 \\ 0 \end{bmatrix} \right\} + \left\{ z^2 \begin{bmatrix} 0 \\ 1 \\ 1 \end{bmatrix} \oplus z^1 \begin{bmatrix} 1 \\ 1 \\ 0 \end{bmatrix} \right\} \pmod{8} \\ &= (4z^6 + 2z^3 + z^0) \begin{bmatrix} 1 \\ 1 \\ 1 \end{bmatrix} + 4 \begin{bmatrix} z^7 \\ z^8 \oplus z^7 \end{bmatrix} + 2 \begin{bmatrix} z^4 \\ z^5 \oplus z^4 \end{bmatrix} \\ &\quad + \begin{bmatrix} z^1 \\ z^2 \oplus z^1 \\ z^2 \end{bmatrix} \pmod{8}. \end{aligned}$$

The reason for this combination of modulo-2 and modulo- M arithmetic is that it reduces the number of logic circuits

required in a signal set mapper. For small lL , it may be simpler to use ROM's for signal set mapping, but for large lL this dual addition becomes preferable. Fig. 7 gives a block diagram of the three 3×8 PSK signal set mappers, and Fig. 8 illustrates the mapper for 4×8 PSK. This combination of modulo-2 and modulo- M addition has no effect on the MSSD's (at least for $L \leq 4$). In a similar manner, we can also obtain the signal set mappers for $L \times 4$ PSK and $L \times 16$ PSK.

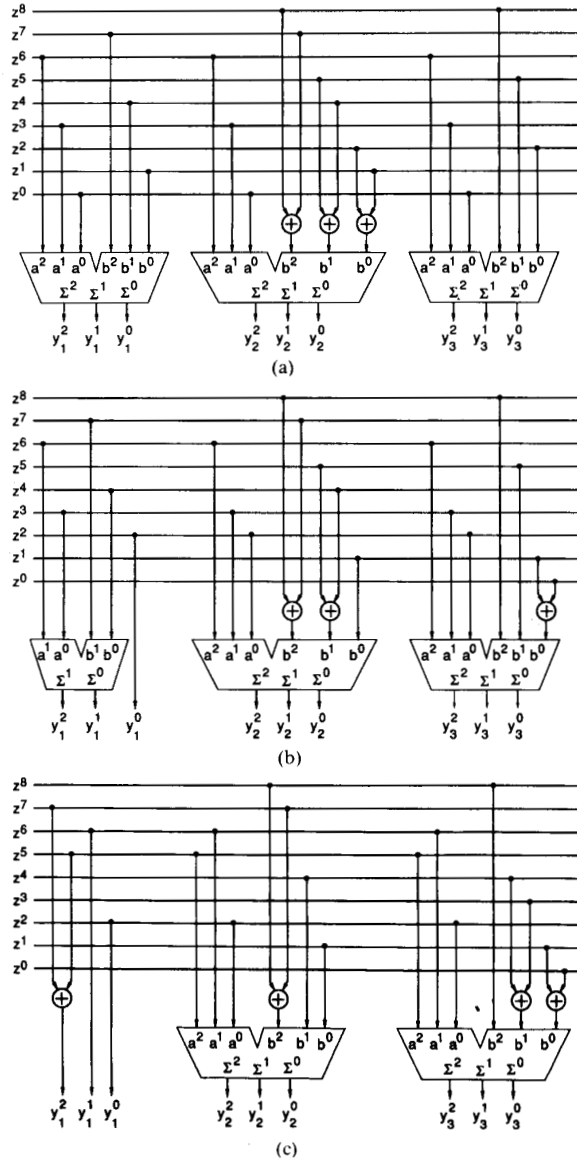
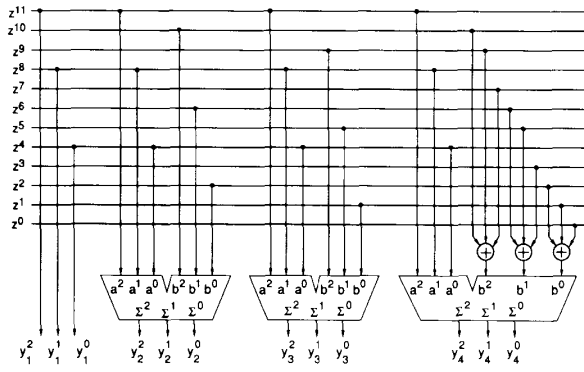


Fig. 7. 3×8 PSK signal set mappers. (a) Mapper (I). (b) Mapper (II). (c) Mapper (III).

Due to the phase rotational properties and simplified hardware that the combined modulo-2 and modulo- M mapping allows, these are the signal sets that are used to find all the trellis codes in this paper.


 Fig. 8. 4×8 PSK signal set mapper.

We have shown that for $q = 0$, the bits that are affected by a phase rotation of Ψ are z^p , for $0 \leq j \leq I-1$. For $q > 0$ the bits that are affected are z^{p-q} , for $0 \leq j \leq I-1$. However, depending on the signal set, $p_j - q$ for some j may be less than zero. If this is true, the minimum phase transparency is $2^{d'}\Psi$, where d' is the number of terms $p_j - q$ that are less than zero, and the number of bits that are affected by a $2^{d'}\Psi$ phase rotation is $s' = I - d'$. For example, the 3×8 PSK signal set in Table III has $p_0 = 0$, $p_1 = 3$, and $p_2 = 6$. Thus if $q = 1$, then $p_0 - q = -1$, which is less than zero, implying that $d' = 1$, and thus only $s' = I - d' = 2$ bits are affected by a $2\Psi = 90^\circ$ phase rotation. (A phase rotation of $\Psi = 45^\circ$ of this signal set produces its coset.)

Fortunately, for the codes and signal sets considered in this paper, the above complication does not occur. This is partly due to the fact that for many signal sets with $q = 0$, the first $L-1$ LSB's are not affected by a phase rotation of Ψ . Since we consider only signal sets with $0 \leq q \leq L-1$, $d' = 0$ in these cases. For those signal sets where this is not true (e.g., in some $3 \times$ MPSK signal sets), it has been found that the convolutional codes produced are inferior (in either d_{free} or number of nearest neighbors) to an alternative signal set with $d' = 0$.

When a signal set is combined with a convolutional encoder we must consider the effect of rotating coded sequences. A similar result to the previously mentioned is obtained so that, depending on the code and the signal set, the signal set can be rotated in multiples of $2^d\Psi$ and still produce valid code sequences (where d defines the degree of transparency). The actual determination of d is de-

scribed in Section III-D. The number of bits that are affected by a $2^d\Psi$ phase rotation is $s = I - d$.

For $0 \leq q \leq L-1$, the actual bits that are affected by a phase rotation of Ψ are z^{b_j} , where $b_j = p_j - q$, for $0 \leq j \leq I-1$. More generally, the bits that are affected by a phase rotation of $2^d\Psi$ are z^{c_j} , where $c_j = p_{j+d} - q$ for $0 \leq j \leq s-1$. These two separate notations (b_j and c_j) are used because the determination of d depends on b_j , as will be shown in Section III-D.

C. The General Encoder System

From the information given thus far, we can now construct a suitable encoder system, as illustrated in Fig. 9. The general encoder system consists of five sections. These sections are the differential precoder, the binary convolutional encoder, the multi-D signal set mapper, the parallel-to-serial converter, and the 2-D signal set mapper. The convolutional encoder is assumed to be in feedback systematic form, as in [1]. That is, $z^j(D) = x^j(D)$ for $1 \leq j \leq k$, where D is the delay operator and polynomial notation is used. The parity sequence, $z^0(D)$, will be some function of itself and the $x^j(D)$, for $1 \leq j \leq k$. The parity check equation of an encoder describes the relationship in time of the encoded bit streams. It is a useful and efficient means of describing high rate convolutional codes, since it represents the input/output encoder relationships in a single equation. For an $R = k/(k+1)$ code, the parity check equation is

$$H^{\tilde{k}}(D)z^{\tilde{k}}(D) \oplus \dots \oplus H^1(D)z^1(D) \oplus H^0(D)z^0(D) = 0(D) \quad (18)$$

where \tilde{k} , $1 \leq \tilde{k} \leq k$, is the number of input sequences checked by the encoder, $H^j(D)$ for $0 \leq j \leq \tilde{k}$ is the parity check polynomial of $z^j(D)$, and $0(D)$ is the all zero sequence.

Since the encoder is systematic, the differential precoder codes only those bits which are affected by a phase rotation. The input bits into the encoder which are precoded are denoted $w^{c_0}, w^{c_1}, \dots, w^{c_{s-1}}$. If $c_0 = 0$, we replace w^0 (which does not exist) by z^0 , as shown in Fig. 9 by the dashed line (a different precoder must then be used). For example, an encoder for a rate $8/9$ code which uses the 3×8 PSK (I) signal set given in Table III-a) may (depending on the phase transparency) need this modification. This is because this signal set has $b_0 = 0$, and thus if the code has $d = 0$, then z^0 will need to be precoded. Fig. 10

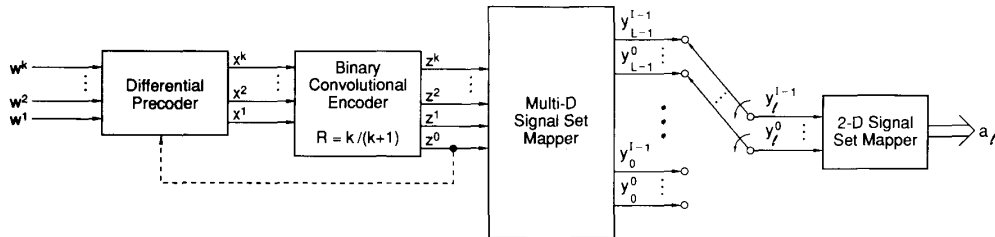


Fig. 9. General encoder system.

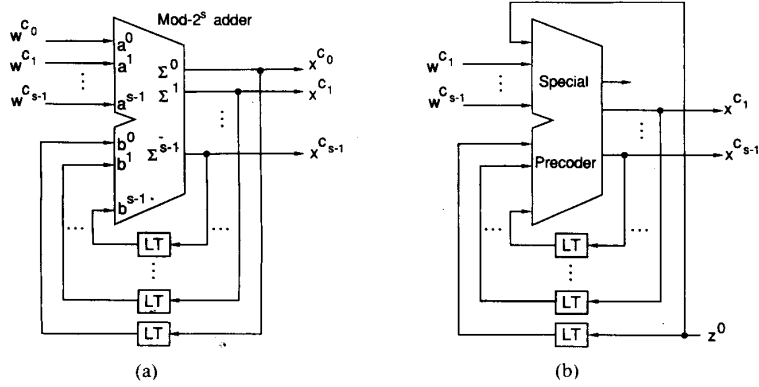


Fig. 10. Differential encoders for general encoder. (a) $C_0 > 0$. (b) $C_0 = 0$.

illustrates the two types of precoders. Note that the storage elements have a delay of LT . Fig. 10(a) illustrates the precoder with $c_0 > 0$, where there are s inputs that are precoded. The basic component of the precoder is the modulo- 2^s adder. For most codes this is the precoder to be used. For the bits that are not precoded, $x^i = w^i$, for $i \neq c_j$.

Fig. 10(b) shows the other case, where $c_0 = 0$ and $s-1$ input bits are precoded (the other precoded bit is z^0). The adder circuit for this case is different from Fig. 10(a), i.e., it is not a modulo- 2^s adder. The Appendix gives the equations for the differential encoder and decoder (for both cases) and an explanation of how these circuits work.

We now summarize the notation and indicate the limits on the parameters used in the search for good codes. For a rate $(IL - q - 1)/(IL - q)$ code,

- I number of bits in each 2-D signal ($2 \leq I \leq 4$),
- M number of signal points in each 2-D signal set,
- L number of 2-D signal sets ($1 \leq L \leq 4$),
- p partition level of signal set ($0 \leq p \leq IL$),
- q partition level p where mapping begins ($0 \leq q \leq L-1$),
- z signal set mapping parameter ($0 \leq z \leq 2^{p-q} - 1$),
- $k = IL - q - 1$ number of input bits to encoder,
- \tilde{k} number of bits checked by encoder ($1 \leq \tilde{k} \leq k$),
- $\Psi = 360^\circ/M$ minimum phase transparency with $q = 0$,
- p_j bits z^{p_j} affected by a Ψ phase rotation with $q = 0$,
- d degree of phase transparency ($2^d \Psi$, for $0 \leq d \leq I$),
- $s = I - d$ number of bits in z affected by a $2^d \Psi$ phase rotation,
- $c_j = p_{j+d} - q$ the bits z^{c_j} affected by a $2^d \Psi$ phase rotation.

There are two types of systematic convolutional encoders that can be constructed. Before proceeding with the description of these encoders, we return to the parity check equation given in (18). As in [1], we define the *constraint*

length v to be the maximum degree of all the parity check polynomials $H^j(D)$, for $0 \leq j \leq \tilde{k}$. For $\tilde{k} < j \leq k$, $H^j(D) = 0$, since the bits corresponding to these polynomials are not checked by the encoder. The parity check polynomials are of the form

$$H^j(D) = 0 \oplus h_{v-1}^j D^{v-1} \oplus \dots \oplus h_1^j D \oplus h_0^j, \quad 1 \leq j \leq \tilde{k} \quad (19a)$$

$$H^0(D) = D^v \oplus h_{v-1}^0 D^{v-1} \oplus \dots \oplus h_1^0 D \oplus 1. \quad (19b)$$

If $\tilde{k} < v$, we let $h_0^j = 0$, for $1 \leq j \leq \tilde{k}$. This insures that the squared Euclidean distance (SED) between paths in a trellis leaving or entering a state is at least Δ_{q+1}^2 . Thus all codes in this class have an MSED between all possible nonparallel coded sequences of at least $2\Delta_{q+1}^2$. The parallel transitions provide an upper bound on the d_{free} of a code. A theoretical justification for constructing codes in this manner can be found in [20] where it is shown, using random coding arguments, that these codes have a large free MSED on the average.

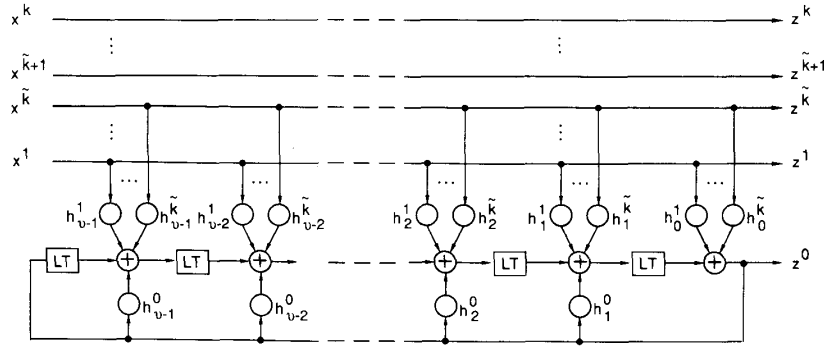
A minimal systematic encoder can be implemented from (19), since $h_0^0 = 1$ [1]. The encoding equations are

$$z^j(D) = x^j(D), \quad 1 \leq j \leq k \quad (20a)$$

$$z^0(D) = H^{\tilde{k}}(D)x^{\tilde{k}}(D) \oplus \dots \oplus H^1(D)x^1(D) \oplus (H^0(D) \oplus 1)z^0(D). \quad (20b)$$

An encoder implementation using (20) is shown in Fig. 11.

For all codes with $v=1$ and for some codes with $v>1$, $\tilde{k} = v$. For these codes we cannot restrict h_0^j , for $1 \leq j \leq \tilde{k}$. This is because \tilde{k} checked bits require at least \tilde{k} terms in $H^j(D)$, for $1 \leq j \leq \tilde{k}$, that are variable. If there are not enough variables, then there will be some nonzero $x^{\tilde{k}} = [x^{\tilde{k}}, \dots, x^2, x^1]$ such that $\sum_{j=1}^{\tilde{k}} H^j(D)x^j = 0 \pmod{2}$. That is, there will be more than $2^{k-\tilde{k}}$ parallel transitions between states in the trellis. To avoid this problem, when $\tilde{k} = v$, we use (19) without any restrictions. In this case, the MSED between all possible nonparallel coded sequences is at least $\Delta_q^2 + \Delta_{q+1}^2$, since the MSED between paths leaving a state is Δ_q^2 (since $h_0^j \in \{0, 1\}$, for $1 \leq j \leq \tilde{k}$) and between paths entering a state is Δ_{q+1}^2 (since $h_v^j = 0$, for $1 \leq j \leq \tilde{k}$).


 Fig. 11. Systematic convolutional encoder with \tilde{k} checked bits.

The multi-D signal set mapper can be implemented as described in Section II-D. We must insure that the correct labels are used to map the signal set if q is greater than zero. All the labels in Figs. 4, 7, and 8 assume that $q = 0$.

The second to last section of the encoder is the parallel to serial converter, which takes the L groups of I bits and forms a stream with I bits in each group. That is, we assume that the channel is limited to transmitting one 2-D signal point at a time. Finally, the 2-D signal set mapper takes the I bits for each 2-D signal point and produces the required real and imaginary (or amplitude and phase) components for a modulator.

Example 3.2: In this example, we describe how to implement a particular code. The code is used with a 3×8 PSK signal set. Thus $L = 3$ and $I = 3$. We also choose $q = 1$, so that a 2.33-bit/T (rate $7/8$) code is formed. The partition that is used is given in Table IV, from which we obtain $p_0 = 2$, $p_1 = 3$, and $p_2 = 6$. The code is 90° transparent, so that $d = 1$ and $s = 2$. Therefore, $c_0 = p_1 - q = 2$, and $c_1 = p_2 - q = 5$. Thus bits w^2 and w^5 are precoded using a modulo-4 adder. Since $c_0 > 0$, the precoder given in Fig. 10(a) is used. For this code, $\tilde{k} = 2$ and the parity check polynomials are $H^0(D) = D^4 \oplus D^2 \oplus D \oplus 1$, $H^1(D) = D$, and $H^2(D) = D^3 \oplus D^2$. Excluding the parallel-to-serial converter and the 2D signal mapper, the encoder is shown in Fig. 12. This code has 16 states ($v = 4$). Note that the

multi-D signal set mapper does not correspond exactly to Fig. 7(b), since $q = 1$.

D. Convolutional Encoder Effects on Transparency

The convolutional encoder can affect the total transparency of the system. The method used to determine transparency is to examine the parity check equation and the bits affected by a phase rotation. A code is transparent if its parity check equation, after substituting $z^j(D)$ with $z^j(D)$ for $0 \leq j \leq \tilde{k}$ (the rotated sequences), remains the same. Normally, at most I bits are affected by a phase rotation i.e., $z^{b_0}, \dots, z^{b_{I-1}}$, $b_j = p_j - q$, for $0 \leq j \leq I - 1$. We have

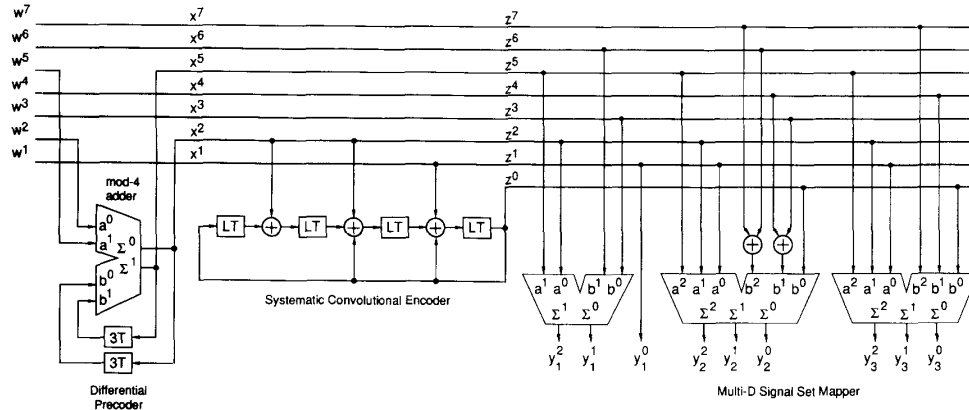
$$z_r^{b_0} = z^{b_0} \oplus 1 \quad (21a)$$

$$z_r^{b_1} = z^{b_1} \oplus z^{b_0} \quad (21b)$$

$$z_r^{b_2} = z^{b_2} \oplus z^{b_0} \cdot z^{b_1} \quad (21c)$$

$$\vdots$$

Assume that the largest value of $b_j \leq \tilde{k}$ is b_0 . This implies that only one term in the parity check equation is affected by a phase rotation. The other bits have no effect since they are not checked by the encoder, i.e., $b_j > \tilde{k}$ for $1 \leq j \leq I - 1$. The parity check equation after a phase rotation


 Fig. 12. Encoder system for rate $7/8$ (2.33 bit/T), 3×8 PSK (I) signal set and 90° transparent code with 16 states and $\tilde{k} = 2$.

of Ψ then becomes

$$\begin{aligned} H^{\tilde{k}}(D)z^{\tilde{k}}(D) \oplus \dots \oplus H^{b_0}(D)[z^{b_0}(D) \oplus 1(D)] \oplus \dots \\ \oplus H^0(D)z^0(D) = 0(D) \\ H^{\tilde{k}}(D)z^{\tilde{k}}(D) \oplus \dots \oplus H^{b_0}(D)z^{b_0}(D) \oplus \dots \\ \oplus H^0(D)z^0(D) = E[H^{b_0}(D)](D) \quad (22) \end{aligned}$$

where $E[H^{b_0}(D)]$ is the modulo-2 number of nonzero terms in $H^{b_0}(D)$ and $1(D) = \sum_{j=-\infty}^{\infty} D^j$ is the all-ones sequence (i.e., $E[H^{b_0}(D)](D) = H^{b_0}(D)1(D)$). Thus, if $H^{b_0}(D)$ has an even number of terms, (22) is the same as (18). That is, the code is transparent to integer multiples of Ψ phase rotations of the signal set. However, if $H^{b_0}(D)$ has an odd number of terms, then $E[H^{b_0}(D)] = 1$ and the coset of the convolutional code is produced. Even though the two equations are closely related, the codes are quite different, and a decoder is not able to produce correctly decoded data from a Ψ phase rotation of the signal set.

Now assume that the first two terms are affected by a phase rotation, i.e., the largest value of $b_j \leq \tilde{k}$ is b_1 . The terms in the parity check polynomial $H^{b_0}(D)z^{b_0}(D) \oplus H^{b_1}(D)z^{b_1}(D)$ now become

$$\begin{aligned} [H^{b_0}(D) \oplus H^{b_1}(D)]z^{b_0}(D) \oplus H^{b_1}(D)z^{b_1}(D) \\ \oplus E[H^{b_0}(D)](D). \end{aligned}$$

In this case the parity check equation is different after a phase rotation (even if $E[H^{b_0}(D)] = 0$). This means that the code is not transparent to a Ψ phase rotation, but it could be transparent to 2Ψ or 4Ψ phase rotations. This is because the phase rotation equations reduce to

$$\begin{aligned} z_r^{b_0} = z^{b_0}, \dots, z_r^{b_{d-1}} = z^{b_{d-1}} \\ z_r^{b_d} = z^{b_d} \oplus 1, z_r^{b_{d+1}} = z^{b_{d+1}} \oplus z^{b_d}, \dots \end{aligned}$$

for a $2^d\Psi$ phase rotation, where $d=1$ or 2 . If $H^{b_1}(D)$ has an even number of terms, then $d=1$. This is because an even number of terms in $H^{b_1}(D)$ cancels the effect on $z^{b_1}(D)$ when the signal set is rotated by 2Ψ . That is, the code is transparent to integer multiples of 2Ψ phase rotations but not to multiples of Ψ . If $H^{b_1}(D)$ has an odd number of terms, this cancellation effect does not occur, implying that $d=2$ and the phase transparency is 4Ψ .

In general, if the largest value of $b_j \leq \tilde{k}$ is b_f , then $d = f + E[H^{b_f}(D)]$. We can then determine those bits z^c which are affected by a $2^d\Psi$ phase rotation, i.e., $c_j = b_{j+d} = p_{j+d} - q$, for $0 \leq j \leq s-1$, where $s = I - d$.

Example 3.3: For the code given in Example 3.2, $\tilde{k} = 2$, $I = 3$, and $q = 1$. Thus $b_0 = 1$, $b_1 = 2$, and $b_2 = 5$. Since the largest value of $b_j \leq 2$ is b_1 , then $f = 1$. Therefore, $d = 1 + E[H^{b_1}(D)] = 1 + E[D^3 \oplus D^2] = 1$. Thus the code is 90° transparent, and $c_0 = 2$ and $c_1 = 5$.

E. Systematic Search for Good Small Constraint Length Codes

An approximate lower bound for the symbol error probability [1] of a multi-D code is given by

$$P_s(e) \geq \frac{N_{\text{free}}}{L} Q \left(\sqrt{\frac{d_{\text{free}}^2 R_{\text{eff}} E_b}{2N_0}} \right) \quad (23)$$

where E_b/N_0 is the energy per information bit to single-sided noise density ratio and $Q(\cdot)$ is the complementary error function. In (23), the division by L normalizes the average number of errors per multi-D signal to that of a 2D signal set.

For each multi-D signal set considered, a number of code rates can be achieved. As v is increased, a comprehensive code search becomes time-consuming due to the greater complexity of each code. We have thus limited our search to $v + \tilde{k} \leq 10$. (The number of checked bits \tilde{k} also affects the complexity of the code search.) As indicated by (23), the criteria used to find the best codes are the free MSE (d_{free}^2) and the number of nearest neighbors (N_{free}). We have also included the code transparency d as a criteria in the code search. The code search algorithm that was implemented is similar to that in [1] but with a number of differences, including the extra criteria mentioned above.

The actual code search involves using a rate $\tilde{k}/(\tilde{k}+1)$ code. Thus two separate notations are used to distinguish the rate $k/(k+1)$ encoder and the simplified rate $\tilde{k}/(\tilde{k}+1)$ encoder. For the rate $k/(k+1)$ encoder, we have $x_n = [x_n^k, \dots, x_n^1]$ (the input to the encoder) and $z_n = [z_n^k, \dots, z_n^1, z_n^0]$ (the mapped bits or encoder output) at time n . Also, $e_n = [e_n^k, \dots, e_n^1, e_n^0]$ is the modulo-2 difference between two encoder outputs z_n and z'_n at time n , i.e., $e_n = z_n \oplus z'_n$. Note that there are 2^{k+1} combinations of z_n and z'_n that give the same e_n . For the rate $\tilde{k}/(\tilde{k}+1)$ code, we denote reduced versions of x_n , z_n , and e_n as $\tilde{x}_n = [\tilde{x}_n^{\tilde{k}}, \dots, \tilde{x}_n^1]$, $\tilde{z}_n = [\tilde{z}_n^{\tilde{k}}, \dots, \tilde{z}_n^1, \tilde{z}_n^0]$, and $\tilde{e}_n = [\tilde{e}_n^{\tilde{k}}, \dots, \tilde{e}_n^1, \tilde{e}_n^0]$, respectively.

To find d_{free} for a particular code, the squared Euclidean weights (SEW) $w^2(e_n)$ are used. As defined in [1], $w^2(e_n)$ is the MSE between all combinations of $a(z_n)$ and $a(z'_n)$ such that $e_n = z_n \oplus z'_n$ and $a(z_n)$ is the actual $L \times \text{MPSK}$ signal point. This can be defined as

$$w^2(e_n) = \min_{\text{all } z_n} d^2[a(z_n), a(z_n \oplus e_n)] \quad (24)$$

where $d^2[a(z_n), a(z'_n)]$ is the SED between $a(z_n)$ and $a(z'_n)$. One can then use the all-zero path as a reference to find d_{free}^2 in a code search, i.e.,

$$d_{\text{free}}^2 = \min_n \sum_n w^2(e_n) \quad (25)$$

where the minimization is over all allowable code sequences with the exception of the all-zero sequence. We can use (25) to find d_{free}^2 provided that the minimization of (24) does not depend on z_n^0 , as shown by Ungerboeck [1].

Although the minimization of (24) does not depend on z_n^0 for $1 \times \text{MPSK}$ signal sets, it cannot be assumed that this also applies to $L \times \text{MPSK}$ for $L \geq 2$. By expressing $d^2[a(z_n), a(z_n \oplus e_n)]$ directly in terms of z_n and e_n , it can be shown that $3 \times 4\text{PSK}$ (I), $3 \times 8\text{PSK}$ (I and II), and $3 \times 16\text{PSK}$ (I, II, and III) all depend on z_n^0 . This implies that (25) becomes a lower bound in these cases. However, due to the large number of parallel transitions for these codes, we can still determine d_{free}^2 (and N_{free}) using a slightly modified version of (25).

Since there are 2^{k+1} values of e_n , a total of 2^{2k+2} computations are required to find all the values of $w^2(e_n)$. For example, a rate 11/12 code with 4×8 PSK modulation requires nearly 17 million computations. This can be reduced by letting $z_n^0 = 0$ (or 1) and minimizing (24) over all $z_n = [z_n^k, \dots, z_n^1, 0]$. This reduces the number of computations to 2^{2k+1} . In fact, it is possible to decrease the number of computations even further. Using some difficult algebraic manipulations, it can be shown that the L output bits z_n^p corresponding to cosets t^p with some components equal to 2^{l-1} can all be set to zero. For example, the 4×8 PSK signal set with $q = 0$ can have bits z_n^7, z_n^9, z_n^{10} , and z_n^{11} all set to zero when minimizing (24). This is due in part to the MPSK signals being antipodal for these values. Thus the total number of computations can be reduced to 2^{2k-L+1} .

To reduce the time needed to find d_{free}^2 , we note that the trellis is equivalent to a rate $\tilde{k}/(\tilde{k}+1)$ code with $2^{k-\tilde{k}}$ parallel transitions. Also, there are $2^{\tilde{k}+1}$ different sets of parallel transitions. If the minimum SEW is found for each of these sets of parallel transitions, the code search is greatly simplified, since the search for a rate $\tilde{k}/(\tilde{k}+1)$ code is all that is needed and \tilde{k} is usually small. Thus the SEW's required for a rate $\tilde{k}/(\tilde{k}+1)$ code search are

$$w^2(\tilde{e}_n) = \min w^2(e_n) \quad (26)$$

where the minimization is over all $[e_n^k, \dots, e_n^{\tilde{k}+1}]$. We define the free MSE of this rate $\tilde{k}/(\tilde{k}+1)$ code as

$$\tilde{d}_{\text{free}}^2 = \min_n \sum w^2(\tilde{e}_n) \quad (27)$$

where the minimization is over all allowable code sequences ($\tilde{e}(D)$) defined by

$$\tilde{e}(D) = \tilde{e}_1 D \oplus \tilde{e}_2 D^2 \oplus \dots \oplus \tilde{e}_N D^N$$

for $\tilde{e}_1, \tilde{e}_N \neq \mathbf{0}$, and $N \geq 2$. The code sequences of length $N = 1$ are the parallel transitions, where the MSE is the MSSD of the parallel transitions. A code might have $\tilde{d}_{\text{free}}^2$ larger than the MSSD of the parallel transitions, implying that d_{free}^2 occurs along the parallel transitions. With k checked bits and a rate $\tilde{k}/(\tilde{k}+1)$ code, the MSSD of the parallel transitions is $\Delta_{q+\tilde{k}+1}^2$. Thus we can express d_{free}^2 as

$$d_{\text{free}}^2 = \min(\tilde{d}_{\text{free}}^2, \Delta_{q+\tilde{k}+1}^2). \quad (28)$$

The best value of \tilde{k} can be determined from the free MSE of the best code for the previous value of v . The search starts with $v = 1$ and $\tilde{k} = 1$, and we find the code with the best d_{free}^2 and N_{free} . We then increase v by one and determine \tilde{k} as follows. If d_{free}^2 for the previous best code was $\tilde{d}_{\text{free}}^2$, then \tilde{k} remains the same. This is because the limit of the parallel transitions $\Delta_{q+\tilde{k}+1}^2$ has not yet been reached and the trellis connectivity needs to be reduced to increase d_{free}^2 or reduce N_{free} . If the previous best code had $d_{\text{free}}^2 = \Delta_{q+\tilde{k}+1}^2$, then \tilde{k} is increased by one from the previous value; otherwise, d_{free}^2 and N_{free} would remain the same. If $\tilde{d}_{\text{free}}^2 = \Delta_{q+\tilde{k}+1}^2$ for the previous best code, then \tilde{k} can remain the same or increase by one. Both values of \tilde{k} should be tried to find the best code. The best

code is then found for this value of v and \tilde{k} , and the above process is repeated for each increasing value of v .

As can be seen from (24), there may be some values of e_n and z_n for which $w^2(e_n) < d^2[a(z_n), a(z_n \oplus e_n)]$. The "number of nearest neighbors" for e_n (denoted $m(e_n)$) is defined as the average number of times that $w^2(e_n)$ equals $d^2[a(z_n), a(z_n \oplus e_n)]$. If $w^2(e_n)$ equals $d^2[a(z_n), a(z_n \oplus e_n)]$ for all values of z_n , then $m(e_n) = 1$. For example, in naturally mapped 8PSK, it is found that for $e_n = [0 \ 1 \ 1]$ and $[1 \ 1 \ 1]$, $d^2[a(z_n), a(z_n \oplus e_n)] = 0.586$ for four values of z_n and 3.414 for the other four values of z_n . Thus $m(e_n) = 0.5$ for $e_n = [0 \ 1 \ 1]$ and $[1 \ 1 \ 1]$. For all other values of e_n , it can be shown that $m(e_n) = 1$. Zehavi and Wolf [21] give a general approach to determining the full code distance spectrum, whereas we are only interested in the number of nearest neighbors.

We can state this generally as follows. Let the number of bits in z_n that are varied to find $w^2(e_n)$ be b . Then

$$m(e_n) = \sum u(w^2(e_n) - d^2[a(z_n), a(z_n \oplus e_n)]) 2^{-b} \quad (29)$$

where $u(\cdot)$ is the unit step function and the summation is over all the bits in z_n that are varied to find $w^2(e_n)$. Normally, $b = k + 1$, but this can be reduced to $b = k - L$ for the reasons mentioned previously.

For the simplified rate $\tilde{k}/(\tilde{k}+1)$ code, $m(\tilde{e}_n)$ is the sum of all the $m(e_n)$ for which $w^2(\tilde{e}_n) = w^2(e_n)$, i.e.,

$$m(\tilde{e}_n) = \sum u(w^2(\tilde{e}_n) - w^2(e_n)) m(e_n) \quad (30)$$

where the summation is over all $[e_n^k, \dots, e_n^{\tilde{k}+1}]$. We can think of $m(\tilde{e}_n)$ as the total average number of nearest neighbors along each set of parallel transitions.

The number of nearest neighbors for the MSSD $\Delta_{q+\tilde{k}+1}^2$ is

$$N_{\Delta} = \sum u(\Delta_{q+\tilde{k}+1}^2 - w^2(e_n)) m(e_n) \quad (31)$$

where the summation is over all $e_n = [e_n^k, \dots, e_n^{\tilde{k}+1}, 0, \dots, 0]$. The number of nearest neighbors for paths with SED $\tilde{d}_{\text{free}}^2$ can be calculated using $m(\tilde{e}_n)$ as follows:

$$\tilde{N}_{\text{free}} = \sum_{\alpha=1}^A \prod_{n=1}^{N_{\alpha}} m(\tilde{e}_n) \quad (32)$$

where N_{α} is the length of a path α that has a SED of $\tilde{d}_{\text{free}}^2$ and A is the number of paths that have a SED of $\tilde{d}_{\text{free}}^2$. If d_{free}^2 occurs along the parallel transitions, $N_{\text{free}} = N_{\Delta}$, and we define the next nearest free SED and number of nearest neighbors as $d_{\text{next}}^2 = \tilde{d}_{\text{free}}^2$ and $N_{\text{next}} = \tilde{N}_{\text{free}}$, respectively. (Note that d_{next}^2 and N_{next} may not be the true next nearest paths, since there may be some closer paths occurring along the parallel transitions.) When there are several codes that have the same free MSE and number of nearest neighbors, the "next nearest" values are used in code selection. When d_{free}^2 occurs along paths with SED $\tilde{d}_{\text{free}}^2$, $N_{\text{free}} = \tilde{N}_{\text{free}}$. The next nearest values in this case are not given in the code tables. If $\tilde{d}_{\text{free}}^2 = \Delta_{q+\tilde{k}+1}^2$, then $N_{\text{free}} = N_{\Delta} + \tilde{N}_{\text{free}}$.

Example 3.4: In Example 3.2 we have a $\tilde{k} = 2$, $q = 1$, rate 7/8 (2.33 bit/T) code with a 3×8 PSK (II) signal set. After determining the mapping of the signal set, (24) was

used to find the SEW's for each signal point. Equation (26) determines the $w^2(\tilde{e}_n)$ used to find the best rate $2/3$ codes. For these codes $d_{\text{free}}^2 = \Delta_{q+\tilde{k}+1}^2 = \Delta_4^2 = 4.0$. Using (31) we determined that N_{free} is 15 (after normalizing, there are only five paths per 2-D symbol). In the code search for the best rate $2/3$ codes, there were many codes that had $d_{\text{next}}^2 = \tilde{d}_{\text{free}}^2 = 4.343$. Thus (32) was used to determine N_{next} for each best code. Table XII gives the values of $w^2(\tilde{e}_n)$ and $m(\tilde{e}_n)$ for each \tilde{e}_n used in the code search. The best code with a transparency of 90° was found to have $N_{\text{next}} = 24$.

TABLE XII
SQUARED EUCLIDEAN WEIGHTS USED IN THE CODE
SEARCH FOR RATE $7/8$ (2.33 BIT/T) CODES
WITH 3×8 PSK (II) AND $\tilde{k} = 2$

\tilde{e}_n	$w^2(\tilde{e}_n)$	$m(\tilde{e}_n)$
000	0.0	1
001	1.172	2
010	1.757	4
011	0.586	1
100	2.0	6
101	1.172	2
110	1.757	4
111	0.586	1

To reduce the number of codes that must be tested in our code search algorithm, rejection rules were used. As in [1, rule 1], time reversal of the parity check polynomials was used to reject codes. Even though $w^2(\tilde{e}_n)$ and $m(\tilde{e}_n)$ are used to find the best codes, [1, rule 2] can still be exploited, provided that $w^2(\tilde{e}_n) = \Delta_{r(\tilde{e}_n)+q}^2$, where $r(\tilde{e}_n)$ is the number of trailing zeros in \tilde{e}_n . When this is not true, it may still be possible to find some combinations of the parity check polynomials that can be rejected (this was also implemented in our code search). Finally, [1, rule 3] was also used to eliminate codes.

In the code search a rate $\tilde{k}/(\tilde{k}+1)$ code is searched for a particular v . Before finding $\tilde{d}_{\text{free}}^2$, the code search program checks to make sure that the code only produces sequences with length $N \geq 2$. If for some input $\tilde{x}_n \neq \mathbf{0}$, the inputs to the systematic encoder are all zero, the state of the encoder goes from one state to the next as if a zero input had occurred. Thus parallel transitions will occur in the rate $\tilde{k}/(\tilde{k}+1)$ code, which should not have parallel transitions. Therefore, codes at level i , $1 \leq i \leq \tilde{k}$, were rejected in the code search if for some $[x^1, \dots, x^1] \neq \mathbf{0}$, $\sum_{j=1}^i x^j H^j(D) \pmod{2} = 0(D)$.

Two programs were used in the code search, one for codes with $v > \tilde{k}$ and the other for codes with $v = \tilde{k}$. For specific values of I , L , and q , $y^q(z)$, for $0 \leq z \leq 2^{IL-q} - 1$, was generated using the coset representative t^p , for $0 \leq p \leq IL - 1$, that are given in Tables VII-IX. The squared Euclidean weights $w^2(e_n)$ were then calculated using (24) for all e_n . Since the value of \tilde{k} can change with each v , $w^2(\tilde{e}_n)$ and $m(\tilde{e}_n)$ were computed, if necessary, as the program went from the smallest to the largest v .

The code search used the various rejection rules before the time consuming tasks of finding $\tilde{d}_{\text{free}}^2$ (using the bidi-

rectional search algorithm [22]) and N_{free} (using a technique based on the Viterbi algorithm). The rejection rules were organized so that the best codes for each of the two possible phase transparencies were found. The code search found those codes that had the largest free distance (for a particular transparency). If a code was found to have its free MSSED equal to or greater than the previous best code, \tilde{N}_{free} was determined, and this code was listed if either its $\tilde{d}_{\text{free}}^2$ or \tilde{N}_{free} had improved over the previous best code.

The octal code generators were then listed along with their $\tilde{d}_{\text{free}}^2$, \tilde{N}_{free} , and phase transparency d . A small list of codes was produced (for each code search) from which the best codes could be chosen. Every time that \tilde{k} is increased by one in the code search (which is done automatically), the program determines and lists $\Delta_{q+\tilde{k}+1}^2$ and N_Δ for use in the code tables.

The asymptotic coding gain γ of each code compared to the uncoded case, as shown in the code tables, is

$$\gamma = 10 \log_{10} (d_{\text{free}}^2 / d_u^2) \quad \text{dB} \quad (33)$$

where d_u^2 is the smallest MSSD of an equivalent uncoded 2-D or multi-D scheme. In nearly all cases, $d_u^2 = \Delta_{q+1}^2$. For codes with a noninteger R_{eff} , no equivalent $1 \times$ MPSK scheme exists which has the same R_{eff} , and so the equivalent uncoded multi-D signal set is used instead. For the 4×8 PSK signal set with $q=3$, $R_{\text{eff}}=2$ bit/T. Thus a natural comparison would be against uncoded 4PSK, which has $d_u^2=2$. (In this case, $\Delta_{q+1}^2=2.343$, which is inconsistent with other codes that also have $R_{\text{eff}}=2$ bit/T.) The asymptotic coding gains compared to uncoded $(M/2)$ -PSK are found by adding to γ the appropriate correction factor

$$\gamma_{M/2} = 10 \log_{10} \left(\frac{R_{\text{eff}} d_u^2}{(I-1) \delta_1^2} \right) \quad \text{dB} \quad (34)$$

as shown in the code tables. The transparency (in degrees) is also given for each code. The parity check polynomials are expressed in octal notation in the code tables, e.g., $H^0(D) = D^6 + D^4 + D^2 + D + 1 \equiv (001 \ 010 \ 111)_2 \equiv (127)_8$.

In Tables XIII, XXIII, and XXXIII codes for TC-1 \times 4PSK (rate $1/2$ 4PSK), TC-1 \times 8PSK (rate $2/3$ 8PSK),

TABLE XIII
TRELLIS-CODED 1×4 PSK^a

v	\tilde{k}	h^1	h^0	Inv.	d_{free}^2	N_{free}	d_{next}^2	N_{next}	γ (dB)
1	1	1	3	360°	6	1	—	—	1.76
2	1	2	5	360°	10	1	—	—	3.98
3	1	06	13	180°	12	2	—	—	4.77
	1	04	13	360°	12	1	—	—	4.77
4	1	06	21	180°	12	1	—	—	4.77
	1	10	23	360°	14	2	—	—	5.44
5	1	36	45	180°	16	2	—	—	6.02
	1	26	53	360°	16	1	—	—	6.02
6	1	042	117	180°	20	11	—	—	6.99
7	1	126	235	180°	20	2	—	—	6.99
	1	144	223	360°	20	1	—	—	6.99
8	1	262	435	180°	24	11	—	—	7.78
	1	362	515	360°	24	9	—	—	7.78
9	1	0644	1123	180°	24	2	—	—	7.78
	1	0712	1047	360°	24	1	—	—	7.78

^a $\gamma_2 = 0$ dB; $R_{\text{eff}} = 1.0$ bit/T, $d_u^2 = 4.0$, $N_u = 1$ (1×2 PSK).

TABLE XIV
 TRELLIS-CODED 2×4 PSK^a

v	\tilde{k}	h^3	h^2	h^1	h^0	Inv.	d_{free}^2	N_{free}	d_{next}^2	N_{next}	γ (dB)
1	1	—	—	1	3	180°	4	2	6	8	0.00
2	2	—	1	3	5	90°	6	6	—	—	1.76
3	2	—	04	06	11	90°	8	5	—	—	3.01
4	2	—	10	06	23	90°	8	1	10	16	3.01
5	3	14	30	02	41	180°	10	8	—	—	3.98
	3	16	24	06	53	360°	10	7	—	—	3.98
6	3	030	042	014	103	180°	12	40.25	—	—	4.77
	3	076	024	010	157	360°	12	30.75	—	—	4.77
7	3	044	022	114	211	180°	12	8	—	—	4.77

^a $\gamma_2 = 1.76$ dB; $R_{\text{eff}} = 1.5$ bit/T, $q = 0$, $d_u^2 = 4$, $N_u = 6$ (2×4 PSK).

and TC- 1×16 PSK (rate $3/4$ 16PSK), respectively, are presented. These tables give the best code for each phase transparency, which (to the best of our knowledge) have not been previously published. The best codes, without regard for phase transparency, were original published by Odenwalder [15] for 4PSK (with the codes in non-systematic form), by Ungerboeck [1], [4] for 8PSK, and Wilson *et al.* [6] for 16PSK.

Tables XIV, XV, XXIV, XXV, XXXIV, and XXXV list the TC- 2×4 PSK codes (rates of 1.5 and 1.0 bit/T), the TC- 2×8 PSK codes (2.5 and 2.0 bit/T), and the TC- 2×16 PSK codes (3.5 and 3.0 bit/T). Tables XVI–XVIII,

 TABLE XV
 TRELLIS-CODED 2×4 PSK^a

v	\tilde{k}	h^2	h^1	h^0	Inv.	d_{free}^2	N_{free}	d_{next}^2	N_{next}	γ (dB)
1	1	—	1	3	90°	8	5	—	—	3.01
2	1	—	2	5	90°	8	1	12	8	3.01
3	2	04	02	11	360°	12	5	—	—	4.77
4	2	14	06	23	180°	12	1	—	—	4.77
5	2	30	16	41	180°	16	8	—	—	6.02
6	2	036	052	115	180°	16	1	—	—	6.02
7	2	044	136	203	180°	20	6	—	—	6.99
8	2	110	226	433	180°	24	33	—	—	7.78

^a $\gamma_2 = 0$ dB; $R_{\text{eff}} = 1.0$ bit/T, $q = 1$, $d_u^2 = 4.0$, $N_u = 1$ (1×2 PSK).

 TABLE XVI
 TRELLIS-CODED 3×4 PSK^a

v	\tilde{k}	h^3	h^2	h^1	h^0	Inv.	d_{free}^2	N_{free}	d_{next}^2	N_{next}	γ (dB)	Signal Set
1	1	—	—	1	3	90°	4	7	6	32	0.00	I
2	2	—	2	1	5	90°	4	3	6	24	0.00	I
	2	—	2	1	5	360°	4	2	—	—	0.00	II
3	2	—	04	02	11	90°	4	1	6	6	0.00	III
	2	—	04	02	11	360°	6	11	—	—	1.76	II
	3	05	04	02	11	90°	4	0.25	—	—	0.00	III
4	2	—	14	02	21	180°	6	6	—	—	1.76	II
3	3	01	02	06	11	360°	6	4	—	—	1.76	II
4	3	10	04	02	21	90°	6	5.5	—	—	1.76	III
	3	12	04	02	21	180°	8	19	—	—	3.01	I
5	3	24	14	02	41	180°	8	7	—	—	3.01	I
6	3	024	042	010	105	180°	8	3	10	16	3.01	I

^a $\gamma_2 = 2.22$ dB; $R_{\text{eff}} = 1.67$ bit/T, $q = 0$, $d_u^2 = 4.0$, $N_u = 15$ (3×4 PSK I).

 TABLE XVII
 TRELLIS-CODED 3×4 PSK^a

v	\tilde{k}	h^3	h^2	h^1	h^0	Inv.	d_{free}^2	N_{free}	d_{next}^2	N_{next}	γ (dB)	Signal Set
1	1	—	—	1	3	90°	4	1	8	4	0.00	III
	1	—	—	1	3	360°	6	7	—	—	1.76	II
2	1	—	—	2	5	360°	6	4	10	9	1.76	II
	2	—	2	1	5	90°	6	2	8	4	1.76	III
	2	—	3	1	5	180°	8	21	—	—	3.01	I
	2	—	2	1	5	360°	8	16	—	—	3.01	II
3	2	—	04	02	11	90°	6	2	8	1	1.76	III
	2	—	02	06	11	180°	8	3	12	100	3.01	II
	3	06	04	03	11	90°	8	1	—	—	3.01	III
4	3	14	04	12	23	90°	10	5	—	—	3.98	III
5	3	30	04	22	43	90°	12	13	—	—	4.77	III
6	3	036	060	026	103	90°	12	2	—	—	4.77	III
7	3	140	160	062	213	90°	12	1	14	5	4.77	III
	3	004	154	056	207	180°	12	1	16	128	4.77	III

^a $\gamma_2 = 1.25$ dB; $R_{\text{eff}} = 1.33$ bit/T, $q = 1$, $d_u^2 = 4.0$, $N_u = 3$ (3×4 PSK II).

TABLE XVIII
TRELLIS-CODED 3×4PSK^a

v	\bar{k}	h^3	h^2	h^1	h^0	Inv.	d_{free}^2	N_{free}	d_{next}^2	N_{next}	γ (dB)	Signal Set
0	0	—	—	—	—	90°	6	4	—	—	1.76	II
1	1	—	—	1	3	90°	6	2	8	1	1.76	III
	1	—	—	1	3	180°	8	3	12	16	3.01	II
2	2	—	3	2	5	90°	10	4	—	—	3.98	III
3	2	—	06	02	11	90°	10	2	—	—	3.98	III
	2	—	02	06	13	180°	12	5	—	—	4.77	III
4	2	—	12	16	21	90°	12	1	14	2	4.77	III
	2	—	04	12	27	180°	12	1	16	22	4.77	III
	3	10	04	02	21	180°	14	3	—	—	5.44	II
5	3	22	16	04	53	180°	16	2	—	—	6.02	II
	3	24	14	02	43	360°	16	1	—	—	6.02	II
6	3	070	004	022	101	180°	18	3	—	—	6.53	II
7	3	156	024	046	213	180°	20	3	—	—	6.99	II
	3	044	014	102	217	360°	20	2	—	—	6.99	II

^a $\gamma_2 = 0.0$ dB; $R_{\text{eff}} = 1.00$ bit/T, $q = 2$, $d_u^2 = 4.0$, $N_u = 1$ (1×2PSK).

XXVI–XXVIII, and XXXVI–XXXVIII list the TC-3×4PSK codes (1.67, 1.33, and 1.0 bit/T), the TC-3×8PSK codes (2.67, 2.33, and 2.0 bit/T), and the TC-3×16PSK codes (3.67, 3.33, and 3.0 bit/T), respectively. Tables XIX–XXIII, XXIX–XXXIII, and XXXIX–XLII list the TC-4×4PSK codes (1.75, 1.5, 1.25, and 1.0 bit/T), the TC-4×8PSK codes (2.75, 2.5, 2.25, and 2.0 bit/T), and the TC-4×16PSK codes (3.75, 3.5, 3.25, and 3.0 bit/T), respectively.

Equivalent $R = 5/6$, TC-2×8PSK (2.5 bit/T) codes with up to 16 states have been found independently by Lafanechère and Costello [8] and by Wilson [9], although with reduced phase transparency. The two-state TC- L ×8PSK and TC- L ×16PSK codes were also found by Divsalar and Simon [23].

TABLE XIX
TRELLIS-CODED 4×4PSK^a

v	\bar{k}	h^3	h^2	h^1	h^0	Inv.	d_{free}^2	N_{free}	d_{next}^2	N_{next}	γ (dB)
1	1	—	—	1	3	90°	4	12	6	64	0.00
2	2	—	2	1	5	90°	4	4	6	48	0.00
3	3	04	02	01	11	90°	6	28	—	—	1.76
4	3	10	04	02	21	90°	8	78	—	—	3.01
5	3	24	14	02	41	90°	8	30	—	—	3.01
6	3	050	032	004	103	90°	8	14	10	160	3.01

^a $\gamma_2 = 2.43$ dB; $R_{\text{eff}} = 1.75$ bit/T, $q = 0$, $d_u^2 = 4.0$, $N_u = 28$ (4×4PSK).

In the code tables it can be seen that, for the same complexity, two codes (and in some cases three codes) are usually given. Note that the code with the worst phase transparency has a better free distance or a lesser number of nearest or next nearest neighbors. Thus, if phase trans-

TABLE XX
TRELLIS-CODED 4×4PSK^a

v	\bar{k}	h^4	h^3	h^2	h^1	h^0	Inv.	d_{free}^2	N_{free}	d_{next}^2	N_{next}	γ (dB)
1	1	—	—	—	1	3	90°	4	4	8	64	0.00
2	2	—	—	2	1	5	90°	8	78	—	—	3.01
3	2	—	—	04	02	11	90°	8	30	—	—	3.01
4	2	—	—	12	04	23	90°	8	16	12	320	3.01
5	3	—	14	34	06	41	90°	8	6	12	176	3.01
	3	—	04	14	22	43	180°	8	6	12	160	3.01
6	4	014	006	056	022	103	90°	8	2	12	62	3.01

^a $\gamma_2 = 1.76$ dB; $R_{\text{eff}} = 1.50$ bit/T, $q = 1$, $d_u^2 = 4.0$, $N_u = 6$ (2×4PSK).

TABLE XXI
TRELLIS-CODED 4×4PSK^a

v	\bar{k}	h^4	h^3	h^2	h^1	h^0	Inv.	d_{free}^2	N_{free}	d_{next}^2	N_{next}	γ (dB)
1	1	—	—	—	1	3	90°	8	30	—	—	3.01
2	1	—	—	—	2	5	90°	8	14	12	64	3.01
3	2	—	—	06	02	11	90°	8	6	12	64	3.01
	2	—	—	02	06	11	180°	8	6	12	32	3.01
	3	—	01	03	06	11	90°	8	2	12	56	3.01
4	3	—	10	14	06	21	90°	8	2	12	8	3.01
5	4	10	04	06	22	41	90°	12	8	—	—	4.77
6	4	024	014	006	042	103	90°	16	109	—	—	6.02

^a $\gamma_2 = 0.97$ dB; $R_{\text{eff}} = 1.25$ bit/T, $q = 2$, $d_u^2 = 4.0$, $N_u = 4$ (4×4PSK).

TABLE XXII
TRELLIS-CODED 4×4PSK^a

v	\tilde{k}	h^3	h^2	h^1	h^0	Inv.	d_{free}^2	N_{free}	d_{next}^2	N_{next}	γ (dB)
0	0	—	—	—	—	90°	8	14	—	—	3.01
1	1	—	—	1	3	180°	8	6	16	64	3.01
2	2	—	2	3	5	90°	8	2	16	64	3.01
3	3	02	04	03	11	90°	16	45	—	—	6.02
4	3	02	10	06	21	90°	16	17	—	—	6.02
5	3	22	10	06	41	90°	16	5	—	—	6.02
6	3	010	060	036	105	90°	16	1	20	4	6.02

^a $\gamma_2 = 0$ dB; $R_{\text{eff}} = 1.00$ bit/T, $q = 3$, $d_u^2 = 4.0$, $N_u = 1$ (1×2PSK).TABLE XXIII
TRELLIS-CODED 1×8PSK^a

v	\tilde{k}	h^2	h^1	h^0	Inv.	d_{free}^2	N_{free}	d_{next}^2	N_{next}	γ (dB)
1	1	—	1	3	180°	2.586	2	—	—	1.12
2	1	—	2	5	180°	4.0	1	4.586	4	3.01
3	2	04	02	11	360°	4.586	2	—	—	3.60
4	2	14	06	23	180°	5.172	4	—	—	4.13
		2	16	04	23	360°	5.172	2.25	—	4.13
5	2	14	26	53	180°	5.172	0.25	—	—	4.13
		2	20	10	45	360°	5.757	2	—	4.59
6	2	074	012	147	180°	6.343	3.25	—	—	5.01
7	2	146	052	225	180°	6.343	0.125	—	—	5.01
		2	122	054	277	360°	6.586	0.5	—	5.18
8	2	146	210	573	180°	7.515	3.375	—	—	5.75
		2	130	072	435	360°	7.515	1.5	—	5.75

^a $\gamma_4 = 0$ dB; $R_{\text{eff}} = 2.0$ bit/T, $d_u^2 = 2.0$, $N_u = 2$ (1×4PSK).

parency is not required, one should choose the less phase transparent code to obtain the maximum performance for a given complexity.

F. Decoder Implementation

When the Viterbi algorithm is used as the decoder, a measure of decoding complexity is given by $2^{v+\tilde{k}}/L$. This is the number of distinct transitions in the trellis diagram

for any TCM scheme normalized to a 2-D signal set. The maximum bit rate of the decoder is kf_d , where f_d is the symbol speed of the decoder. Since k is quite large for multi-D signal sets (at least $(I-1)L$), high bit rates can be achieved. For example, a Viterbi decoder has been constructed for a rate 7/9 periodically time-varying trellis code (PTVTC) with $v=4$, $\tilde{k}=2$, and 8PSK modulation [24]. This decoder has $f_d=60$ MHz and a bit rate of 140 Mbit/s. However, with the equivalent rate 7/8 code with 3×8PSK modulation, the bit rate will be $L=3$ times as fast, i.e., 420 Mbit/s. The branch metric calculator, though, will be more complicated due to the larger number of parallel transitions between states. Alternatively, one could build a decoder operating at a 20 MHz speed and achieve the same bit rate of 140 Mbit/s. In addition to providing decreased decoder complexity, this multi-D code has an asymptotic coding gain which is 0.56 dB greater and is 90° transparent, compared with a 180° transparency for the PTVTC [25].

Although the decoding complexity of the Viterbi algorithm is measured in terms of $2^{v+\tilde{k}}/L$, for multi-D schemes the complexity of subset (parallel transition) decoding must also be taken into account due to the large number of parallel transitions.

The Viterbi decoder must find which of the $2^{k-\tilde{k}}$ parallel transitions is closest, in a maximum likelihood sense, to the received signal. A brute-force method would be to determine the metric for each of the $2^{k-\tilde{k}}$ paths and then find the minimum. This would involve at least $2^{k-\tilde{k}}-1$ comparisons. Since there are $2^{\tilde{k}+1}$ sets of parallel transitions, a total of $2^{k+1}-2^{\tilde{k}+1}$ comparisons would be required. For large k and small \tilde{k} , this is an unacceptably large number of computations.

Fortunately, as shown in [13] for binary lattices, it is possible to reduce greatly the number of computations

TABLE XXIV
TRELLIS-CODED 2×8PSK^a

v	\tilde{k}	h^3	h^2	h^1	h^0	Inv.	d_{free}^2	N_{free}	d_{next}^2	N_{next}	γ (dB)	
1	1	—	—	1	3	90°	1.757	8	2.0	4	1.76	
2	1	—	—	2	5	90°	2.0	4	2.929	32	2.32	
3	2	—	04	06	11	45°	2.929	16	—	—	3.98	
4	2	—	16	12	23	45°	3.515	56	—	—	4.77	
5	2	—	10	06	41	45°	3.515	16	—	—	4.77	
6	2	—	004	030	113	45°	4.0	6	4.101	80	5.33	
		2	—	044	016	107	90°	4.0	6	4.101	48	5.33
7	3	110	044	016	317	90°	4.0	2	4.101	25	5.33	

^a $\gamma_4 = -1.35$ dB; $R_{\text{eff}} = 2.5$ bit/T, $q = 0$, $d_u^2 = 1.172$, $N_u = 4$ (2×8PSK).TABLE XXV
TRELLIS-CODED 2×8PSK^a

v	\tilde{k}	h^3	h^2	h^1	h^0	Inv.	d_{free}^2	N_{free}	d_{next}^2	N_{next}	γ (dB)
1	1	—	—	1	3	45°	3.172	8	4.0	6	2.00
2	1	—	—	2	5	45°	4.0	6	5.172	32	3.01
3	2	—	04	02	11	180°	4.0	2	5.172	16	3.01
4	3	04	14	02	21	90°	5.172	8	—	—	4.13
5	3	24	14	06	43	90°	6.0	6	—	—	4.77
6	3	012	050	004	125	90°	6.343	5.5	—	—	5.01
7	3	110	044	016	317	90°	7.515	25	—	—	5.75

^a $\gamma_4 = 0$ dB; $R_{\text{eff}} = 2.0$ bit/T, $q = 1$, $d_u^2 = 2.0$, $N_u = 2$ (1×4PSK).

TABLE XXVI
TRELLIS-CODED 3×8PSK^a

v	\tilde{k}	h^3	h^2	h^1	h^0	Inv.	d_{free}^2	N_{free}	d_{next}^2	N_{next}	γ (dB)	Signal Set
1	1	—	—	1	3	45°	1.172	4	—	—	0.00	II
2	1	—	—	2	5	45°	1.757	16	—	—	1.76	II
3	2	—	04	02	11	45°	2.0	6	2.343	16	2.32	I
4	3	14	04	02	21	90°	2.343	12	—	—	3.01	I
	3	10	04	02	21	180°	2.343	8	—	—	3.01	I
5	3	30	14	02	53	90°	2.929	48	—	—	3.98	I
6	3	050	022	006	103	90°	3.172	12	—	—	4.33	I
7	3	056	112	004	225	90°	3.515	84	—	—	4.77	I
	3	100	050	022	255	180°	3.515	76	—	—	4.77	I

^a $\gamma_4 = -1.07$ dB; $R_{\text{eff}} = 2.67$ bit/T, $q = 0$, $d_u^2 = 1.172$, $N_u = 12$ (3×8PSK I).

TABLE XXVII
TRELLIS-CODED 3×PSK^a

v	\tilde{k}	h^4	h^3	h^2	h^1	h^0	Inv.	d_{free}^2	N_{free}	d_{next}^2	N_{next}	γ (dB)	Signal Set
1	1	—	—	—	1	3	90°	2.0	6	2.343	16	0.56	II
2	2	—	—	—	3	1	90°	2.586	6	—	—	1.68	II
3	2	—	—	06	02	11	90°	3.515	16	—	—	3.01	II
	2	—	—	04	02	11	180°	3.757	24	—	—	3.30	II
4	3	—	10	04	06	21	45°	3.757	12	—	—	3.30	III
	2	—	—	14	02	27	90°	4.0	15	4.343	24	3.57	II
5	3	—	22	16	06	41	45°	4.0	7	—	—	3.57	III
6	3	—	010	046	060	105	45°	4.0	3	4.686	8	3.57	III
	4	060	024	014	002	101	180°	4.0	2	—	—	3.57	III

^a $\gamma_4 = 0.11$ dB; $R_{\text{eff}} = 2.33$ bit/T, $q = 1$, $d_u^2 = 1.757$, $N_u = 8$ (3×8PSK II).

TABLE XXVIII
TRELLIS-CODED 3×8PSK^a

v	\tilde{k}	h^4	h^3	h^2	h^1	h^0	Inv.	d_{free}^2	N_{free}	d_{next}^2	N_{next}	γ (dB)	Signal Set
1	1	—	—	—	1	3	180°	3.757	24	—	—	2.74	II
2	1	—	—	—	2	5	180°	4.0	15	5.757	144	3.01	II
3	2	—	—	04	02	11	45°	4.0	7	—	—	3.01	III
4	2	—	—	12	04	27	45°	4.0	3	5.757	32	3.01	III
5	3	—	14	24	02	41	180°	5.757	17.5	—	—	4.59	III
	3	—	16	22	06	53	360°	5.757	17	—	—	4.59	III
6	3	—	030	042	014	103	180°	6.0	11	—	—	4.77	III
	4	014	044	024	006	103	180°	6.0	4	—	—	4.77	II

^a $\gamma_4 = 0$ dB; $R_{\text{eff}} = 2.00$ bit/T, $q = 2$, $d_u^2 = 2.0$, $N_u = 2$ (1×4PSK).

TABLE XXIX
TRELLIS-CODED 4×8PSK^a

v	\tilde{k}	h^4	h^3	h^2	h^1	h^0	Inv.	d_{free}^2	N_{free}	d_{next}^2	N_{next}	γ (dB)
1	1	—	—	—	1	3	45°	1.172	8	1.757	64	0.00
2	2	—	—	—	2	1	45°	1.757	48	—	—	1.76
3	2	—	—	04	02	11	45°	2.0	8	2.343	64	2.32
4	3	—	10	04	02	21	45°	2.343	40	—	—	3.01
5	3	—	30	14	02	41	45°	2.343	8	2.929	288	3.01
6	4	030	020	052	014	101	45°	2.929	136	—	—	3.98

^a $\gamma_4 = -0.94$ dB; $R_{\text{eff}} = 2.75$ bit/T, $q = 0$, $d_u^2 = 1.172$, $N_u = 24$ (4×8PSK).

TABLE XXX
TRELLIS-CODED 4×8PSK^a

v	\tilde{k}	h^3	h^2	h^1	h^0	Inv.	d_{free}^2	N_{free}	d_{next}^2	N_{next}	γ (dB)	
1	1	—	—	1	3	45°	2.0	8	2.343	64	2.32	
2	2	—	—	2	1	5	45°	2.343	40	—	—	3.01
3	2	—	04	02	11	45°	2.343	8	3.172	32	3.01	
4	3	14	04	02	21	45°	3.172	16	—	—	4.33	
5	3	24	14	02	41	45°	3.515	64	—	—	4.77	
6	3	014	024	042	103	45°	4.0	28	4.686	1088	5.33	

^a $\gamma_4 = -1.35$ dB; $R_{\text{eff}} = 2.50$ bit/T, $q = 1$, $d_u^2 = 1.172$, $N_u = 4$ (2×8PSK).

TABLE XXXI
TRELLIS-CODED 4×8 PSK^a

v	\tilde{k}	h^4	h^3	h^2	h^1	h^0	Inv.	d_{free}^2	N_{free}	d_{next}^2	N_{next}	γ (dB)
1	1	—	—	—	1	3	45°	2.343	8	3.172	32	0.69
2	2	—	—	3	1	5	45°	3.172	16	—	—	2.00
3	2	—	—	06	02	11	45°	4.0	28	4.343	64	3.01
	2	—	—	02	06	11	90°	4.0	28	4.686	64	3.01
4	3	—	04	06	12	21	45°	4.0	12	4.686	32	3.01
5	4	10	04	06	22	41	45°	4.0	4	4.686	16	3.01

^a $\gamma_4 = 0.51$ dB; $R_{\text{eff}} = 2.25$ bit/T, $q = 2$, $d_u^2 = 2.0$, $N_u = 8$ (4×8 PSK).TABLE XXXII
TRELLIS-CODED 4×8 PSK^a

v	\tilde{k}	h^4	h^3	h^2	h^1	h^0	Inv.	d_{free}^2	N_{free}	d_{next}^2	N_{next}	γ (dB)
1	1	—	—	—	1	3	90°	4.0	28	4.686	64	3.01
2	2	—	—	2	3	5	45°	4.0	12	4.686	32	3.01
3	3	—	02	04	03	11	45°	4.0	4	4.686	16	3.01
4	4	10	04	02	03	21	45°	4.686	8	—	—	3.70
5	4	02	10	04	22	41	45°	6.343	16	—	—	5.01
6	4	034	044	016	036	107	45°	6.686	6	—	—	5.24
	4	044	024	014	016	103	90°	7.029	24	—	—	5.46

^a $\gamma_4 = 0$ dB; $R_{\text{eff}} = 2.00$ bit/T, $q = 3$, $d_u^2 = 2.0$, $N_u = 2$ (1×4 PSK).TABLE XXXIII
TRELLIS-CODED 1×16 PSK^a

v	\tilde{k}	h^2	h^1	h^0	Inv.	d_{free}^2	N_{free}	d_{next}^2	N_{next}	γ (dB)
1	1	—	1	3	90°	0.738	2	—	—	1.00
2	1	—	2	5	90°	1.324	4	—	—	3.54
3	1	—	06	13	45°	1.476	8	—	—	4.01
	1	—	04	13	90°	1.476	4	—	—	4.01
4	1	—	06	21	45°	1.476	4	—	—	4.01
	1	—	10	23	90°	1.628	4	—	—	4.44
5	1	—	24	43	45°	1.781	8	—	—	4.83
	1	—	10	45	90°	1.910	8	—	—	5.13
6	1	—	056	135	45°	2.0	2	2.085	16	5.33
	1	—	032	107	90°	2.0	2	2.085	8	5.33
7	1	—	126	235	45°	2.0	2	2.366	16	5.33
8	2	344	162	717	90°	2.085	2.938	—	—	5.51
	2	224	112	527	180°	2.085	1.219	—	—	5.51

^a $\gamma_8 = 0$ dB; $R_{\text{eff}} = 3.0$ bit/T, $d_u^2 = 0.586$, $N_u = 2$ (1×8 PSK).TABLE XXXIV
TRELLIS-CODED 2×16 PSK^a

v	\tilde{k}	h^2	h^1	h^0	Inv.	d_{free}^2	N_{free}	d_{next}^2	N_{next}	γ (dB)
1	1	—	1	3	45°	0.457	8	—	—	1.76
2	1	—	2	5	45°	0.586	4	0.761	32	2.84
3	2	04	06	11	22.5°	0.761	16	—	—	3.98
4	2	16	12	23	22.5°	0.913	56	—	—	4.77
5	2	10	06	41	22.5°	0.913	16	—	—	4.77
6	2	004	030	113	22.5°	1.066	80	—	—	5.44
	2	044	016	107	45°	1.066	48	—	—	5.44
7	2	074	132	217	22.5°	1.172	4	1.218	228	5.85

^a $\gamma_8 = -2.17$ dB; $R_{\text{eff}} = 3.5$ bit/T, $q = 0$, $d_u^2 = 0.304$, $N_u = 4$ (2×16 PSK).TABLE XXXV
TRELLIS-CODED 2×16 PSK^a

v	\tilde{k}	h^3	h^2	h^1	h^0	Inv.	d_{free}^2	N_{free}	d_{next}^2	N_{next}	γ (dB)
1	1	—	—	1	3	22.5°	0.890	8	—	—	1.82
2	1	—	—	2	5	22.5°	1.172	4	1.476	32	3.01
3	2	—	04	02	11	90°	1.476	16	—	—	4.01
4	2	—	14	06	23	45°	1.757	8	—	—	4.77
5	2	—	30	16	41	45°	1.781	16	—	—	4.83
6	2	—	044	016	107	45°	2.0	4	2.085	48	5.33
7	3	110	044	016	317	45°	2.085	25	—	—	5.51

^a $\gamma_8 = 0$ dB; $R_{\text{eff}} = 3.0$ bit/T, $q = 1$, $d_u^2 = 0.586$, $N_u = 2$ (1×8 PSK).

TABLE XXXVI
TRELLIS-CODED 3 × 16PSK^a

v	\bar{k}	h^3	h^2	h^1	h^0	Inv.	d_{free}^2	N_{free}	d_{next}^2	N_{next}	γ (dB)	Signal Set
1	1	—	—	1	3	22.5°	0.304	4	—	—	0.00	II
2	1	—	—	2	5	22.5°	0.457	16	—	—	1.76	II
3	2	—	04	02	11	22.5°	0.586	6	0.609	16	2.84	I
4	3	14	04	02	21	45°	0.609	12	—	—	3.01	I
	3	10	04	02	21	90°	0.609	8	—	—	3.01	I
5	3	30	14	02	53	45°	0.761	48	—	—	3.98	I
6	3	050	022	006	103	45°	0.890	12	—	—	4.66	I
7	3	056	112	004	225	45°	0.913	84	—	—	4.77	I
	3	100	050	022	255	90°	0.913	76	—	—	4.77	I

^a $\gamma_R = 0$ dB; $R_{eff} = 3.67$ bit/T, $q = 0$, $d_u^2 = 0.304$, $N_u = 12$ (3 × 16PSK I).

TABLE XXXVII
TRELLIS-CODED 3 × 16PSK^a

v	\bar{k}	h^3	h^2	h^1	h^0	Inv.	d_{free}^2	N_{free}	d_{next}^2	N_{next}	γ (dB)	Signal Set
1	1	—	—	1	3	45°	0.586	6	0.609	16	1.08	II
2	2	—	3	1	7	45°	0.738	6	—	—	2.08	II
3	2	—	06	02	11	45°	0.913	16	—	—	3.01	II
	2	—	04	02	11	90°	1.043	24	—	—	3.58	II
4	3	10	04	06	21	22.5°	1.043	12	—	—	3.58	III
	2	—	14	02	27	45°	1.172	12	1.195	24	4.09	II
5	3	34	16	06	41	22.5°	1.172	4	—	—	4.09	III
6	3	032	046	006	103	22.5°	1.218	8	—	—	4.26	III
7	3	014	102	044	203	22.5°	1.370	32	—	—	4.77	III
	3	006	072	062	223	45°	1.476	8	—	—	5.09	III

^a $\gamma_R = -1.97$ dB; $R_{eff} = 3.33$ bit/T, $q = 1$, $d_u^2 = 0.457$, $N_u = 8$ (3 × 16PSK II).

TABLE XXXVIII
TRELLIS-CODED 3 × 16PSK^a

v	\bar{k}	h^3	h^2	h^1	h^0	Inv.	d_{free}^2	N_{free}	d_{next}^2	N_{next}	γ (dB)	Signal Set
1	1	—	—	1	3	90°	1.043	24	—	—	2.50	II
2	1	—	—	2	5	90°	1.172	12	1.628	144	3.01	II
3	2	—	04	02	11	22.5°	1.172	4	—	—	3.01	III
4	2	—	12	04	27	22.5°	1.628	32	—	—	4.44	III
5	2	—	14	02	41	22.5°	1.628	16	—	—	4.44	III
	2	—	22	14	43	45°	1.757	16	—	—	4.77	III
6	2	—	054	020	115	22.5°	1.757	8	2.085	48	4.77	III
	3	020	004	012	101	45°	2.0	6	2.085	72	5.33	II
	3	050	030	026	101	90°	2.0	6	2.085	60	5.33	II
7	3	060	106	050	213	45°	2.0	6	2.214	56	5.33	III
	3	016	110	052	203	90°	2.0	6	2.343	64	5.33	III

^a $\gamma_R = 0$ dB; $R_{eff} = 3.00$ bit/T, $q = 2$, $d_u^2 = 0.586$, $N_u = 2$ (1 × 8PSK).

TABLE XXXIX
TRELLIS-CODED 4 × 16PSK^a

v	\bar{k}	h^4	h^3	h^2	h^1	h^0	Inv.	d_{free}^2	N_{free}	d_{next}^2	N_{next}	γ (dB)
1	1	—	—	—	1	3	22.5°	0.304	8	0.457	64	0.00
2	2	—	—	2	1	5	22.5°	0.457	48	—	—	1.76
3	2	—	—	04	02	11	22.5°	0.586	8	0.609	64	2.84
4	3	—	10	04	02	21	22.5°	0.609	40	—	—	3.01
5	3	—	30	14	02	41	22.5°	0.609	8	0.761	288	3.01
6	4	030	020	052	014	101	22.5°	0.761	136	—	—	3.98

^a $\gamma_R = -1.87$ dB; $R_{eff} = 3.75$ bit/T, $q = 0$, $d_u^2 = 0.304$, $N_u = 24$ (4 × 16PSK).

TABLE XL
TRELLIS-CODED 4 × 16PSK^a

v	\bar{k}	h^3	h^2	h^1	h^0	Inv.	d_{free}^2	N_{free}	d_{next}^2	N_{next}	γ (dB)
1	1	—	—	1	3	22.5°	0.586	8	0.609	64	2.84
2	2	—	—	2	1	5	22.5°	0.609	40	—	3.01
3	2	—	04	02	11	22.5°	0.609	8	0.890	32	3.01
4	3	14	04	02	21	22.5°	0.890	16	—	—	4.66
5	3	24	14	02	41	22.5°	0.913	64	—	—	4.77
6	3	014	024	042	103	22.5°	1.172	24	1.218	1088	5.85

^a $\gamma_R = -2.17$ dB; $R_{eff} = 3.50$ bit/T, $q = 1$, $d_u^2 = 0.304$, $N_u = 4$ (2 × 16PSK).

TABLE XLI
 TRELLIS-CODED 4×16 PSK^a

v	\tilde{k}	h^4	h^3	h^2	h^1	h^0	Inv.	d_{free}^2	N_{free}	d_{next}^2	N_{next}	γ (dB)
1	1	—	—	—	1	3	22.5°	0.609	8	0.890	32	0.17
2	2	—	—	3	1	5	22.5°	0.890	16	—	—	1.82
3	2	—	—	06	02	11	22.5°	1.172	24	1.195	64	3.01
2	—	—	—	02	06	11	45.0°	1.172	24	1.218	64	3.01
4	3	—	04	06	12	21	22.5°	1.172	8	1.218	32	3.01
5	4	10	04	06	22	41	22.5°	1.218	16	—	—	3.18
6	4	050	030	024	016	101	22.5°	1.499	72	—	—	4.08

^a $\gamma_k = 0.35$ dB; $R_{\text{eff}} = 3.25$ bit/T, $q = 2$, $d_u^2 = 0.586$, $N_u = 8$ (4×16 PSK).

 TABLE XLII
 TRELLIS-CODED 4×16 PSK^a

v	\tilde{k}	h^3	h^2	h^1	h^0	Inv.	d_{free}^2	N_{free}	d_{next}^2	N_{next}	γ (dB)	
1	1	—	—	1	3	45°	1.172	24	1.218	64	3.01	
2	2	—	—	2	3	5	22.5°	1.172	8	1.218	32	3.01
3	3	02	04	03	11	22.5°	1.218	16	—	—	3.18	
4	3	04	10	06	21	22.5°	1.781	48	—	—	4.83	
5	3	22	16	06	41	22.5°	1.804	24	—	—	4.88	
3	—	24	14	02	43	45°	1.827	64	—	—	4.94	
6	3	050	024	006	103	22.5°	2.0	8	2.343	64	5.33	

^a $\gamma_k = 0$ dB; $R_{\text{eff}} = 3.00$ bit/T, $q = 3$, $d_u^2 = 0.586$, $N_u = 2$ (1×8 PSK).

required. In fact, the decoding scheme becomes very similar to Viterbi decoding except that finite length sequences are used.

To illustrate this we will present the decoding scheme for TC- 2×8 PSK parallel transitions with $\tilde{k} = 2$ and an efficiency of 2.5 bit/T (a rate 5/6 code). There are eight sets of parallel transitions, with eight paths in each set. Fig. 13 shows the parallel transition decoding trellis for $\tilde{z} = [0 \ 0 \ 0]$ (i.e., the LSB's are set to zero). In Fig. 1 we use the notation A0 to indicate the whole 8PSK signal set, which divides into B0 and B1 (4PSK signal sets rotated 45° from each other). B0 divides into C0 and C2 (2PSK signal sets rotated 90° from each other), and B1 divides into C1 and C3. This notation is also used in [1] for partitioning an 8PSK signal set. Each segment in Fig. 13 thus represents two parallel lines. The length of this trellis equals the dimensionality $L = 2$ of the signal set.

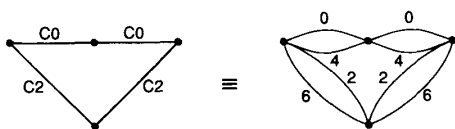


Fig. 13. Parallel transition decoding trellis for $\tilde{z} = [0 \ 0 \ 0]$ and 2×8 PSK signal set.

The path $C0 \times C0$ corresponds to those four paths that have $z^3 = 0$ and $C2 \times C2$ corresponds to those four paths that have $z^3 = 1$, giving a total of eight paths. To decode, hard decisions can be made for C0 and C2 for each time period, from which the values of z^4 and z^5 can be determined. For example, say that $C0 \times C0$ decodes into the points 04, with a metric of m_0 , and $C2 \times C2$ decodes into the points 66, with a metric of m_1 , where the metrics are the sum of the Euclidean distances (or log-likelihood met-

rics for a quantized channel) from the first and second received points. After comparing the two metrics, if $m_0 < m_1$, then $z^3 = 0$ and the point 04 would give $z^4 = 1$ and $z^5 = 0$ (see Table I). If $m_0 > m_1$, then $z^3 = 1$, and the point 66 would give $z^4 = 0$ and $z^5 = 1$. This is equivalent to the add-compare-select (ACS) operation within a Viterbi decoder.

To decode the other sets of parallel transitions, the cosets formed by z^0 , z^1 , and z^2 can be added to the trellis paths $C0 \times C0$ and $C2 \times C2$ to form the required trellis. This is illustrated in Fig. 14, where the ending state in the trellis indicates which set of parallel transitions is being decoded. This example involves a total of eight hard comparisons and eight ACS-type comparisons. These 16 comparisons compare with the 56 comparisons required in a brute force approach, a 3.5 times reduction.

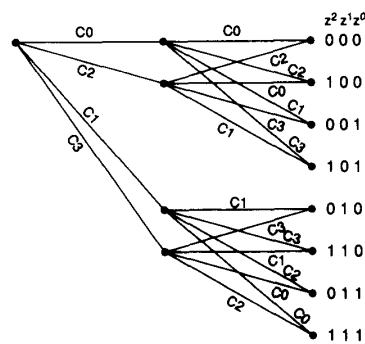


Fig. 14. Full parallel transition decoding trellis for 2×8 PSK signal set.

The above maximum likelihood method can be applied to other codes where a Viterbi-like decoder can be used to decode the parallel transitions. With this method the complexity of decoding the parallel transitions can approach

the complexity of the rate $\tilde{k}/(\tilde{k}+1)$ Viterbi decoder. A simpler approach may be with large lookup tables using ROM's. The ROM itself would output the $k-\tilde{k}$ bits of the chosen path, along with the branch metric for that path. For the TC-2 \times PSK example given previously, we could use one ROM for each of parallel transitions. If the ROM's had 8-bit words, then three bits could be used for the decision, and the remaining five bits for the branch metric. A total of eight ROM's would then be required, one for each set of the parallel transitions.

When using ROM's, it is desirable to reduce the number of bits b required to represent each received 2-D signal point, since there are a total of bL bits required to address the ROM. One way to reduce b is to convert the "checkerboard" (rectangular) type decision boundaries that result from separate quantization of the in-phase I and quadrature Q components to "dartboard" (radial) type decision boundaries. For example, if four bits are used in I and Q for an 8PSK signal with checkerboard decision boundaries, a dartboard pattern as shown in Fig. 15 may be used instead with a total of five bits to represent each point (a reduction of three bits). A ROM may be used to do the conversion, or the dartboard pattern already may be available as polar coordinates from a digital demodulator.

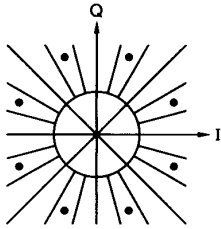


Fig. 15. Dartboard decision boundaries for 8PSK (32 regions).

A problem with TC- $L \times$ MPSK is the need to synchronize the decoder with the L 2-D symbols on each trellis branch. For $q=0$, most codes are fully transparent. The decoder performance can then be used to find the correct synchronization with the received sequence. For $q>0$, many codes are not fully transparent, and the decoder will need to synchronize to one of the $2^d L$ possibilities (which can be quite large for some codes). However, one can take advantage of the fact that not all signal points are used for $q>0$. For example, the 2 \times 8PSK signal set with $q=1$ consists of the signal sets $B_0 \times B_0$ or $B_1 \times B_1$. The synchronizer would find the smallest distance between a received pair of points and the expected signal set. These distances would then be accumulated over a sufficient length of time to make a reliable decision on the symbol timing.

If we let each signal point be represented by its phase (since the amplitude is constant for 8PSK), we can write $B_0 = \{0^\circ, 90^\circ, 180^\circ, 270^\circ\}$, and $B_1 = \{45^\circ, 135^\circ, 225^\circ, 315^\circ\}$. Let ϕ_n^1 and ϕ_n^2 represent the phase of the first and second received symbols, respectively. The synchronizer distance metric is then given by

$$\Phi_n = \min_{i \in \{0,1\}} \left(\min_{\alpha \in B_i} |\phi_n^1 - \alpha| + \min_{\beta \in B_i} |\phi_n^2 - \beta| \right).$$

In the synchronized noiseless case, Φ_n will equal zero. In the nonsynchronized noiseless case, there are two possible outcomes for Φ_n , i.e., complete matchup ($\Phi_n = 0^\circ$) and only one signal is matched ($\Phi_n = 45^\circ$). If each possibility is equally likely, then the average value of Φ_n is 22.5° . With noise, Φ_n can be accumulated over a sufficient length of symbols to take advantage of this average phase distance between the nonsynchronized and synchronized cases to determine symbol synchronization reliably. This symbol synchronization is independent of the Viterbi decoder, so the decoder must only determine phase synchronization.

G. Discussion

To make a comparison of all the codes listed, a plot of nominal coding gain $\gamma^* = 10 \log_{10} d_{\text{free}}^2$ versus complexity ($\beta = \log_2(2^{v+k}/L) = v + \tilde{k} - \log_2 L$) for each code found is made. These plots are given in Fig. 16 for effective rates of 1.0 (with 4PSK modulation), 2.0 (8PSK), and 3.0 bit/T (16PSK), Fig. 17 for effective rates of 1.5 (4PSK), 2.5 (8PSK), and 3.5 bit/T (16PSK), and Fig. 18 (for the remaining rates). (Note that these graphs do not take into account the additional complexity due to parallel transitions.) Some one-state ("uncoded") codes are included as well. These one-state codes correspond to block-coded (or multilevel) schemes that have recently become an active research area [26]–[34]. Although the multi-D one-state codes have negative complexity (compared to trellis codes), they can achieve coding gains above 0 dB.

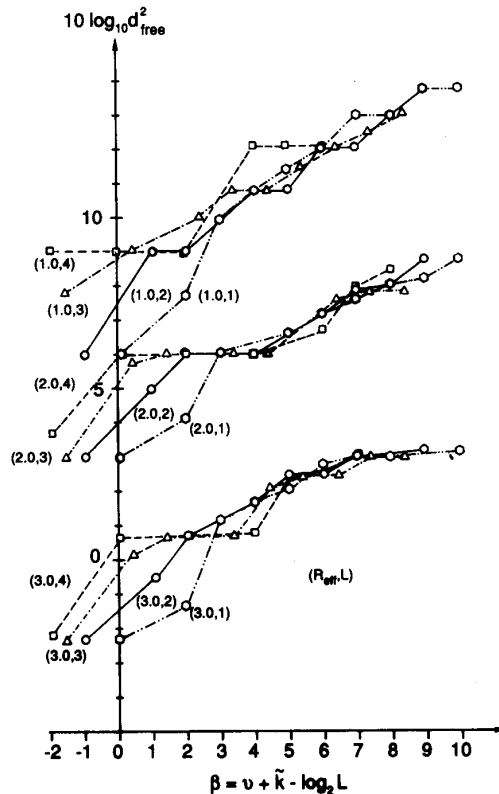


Fig. 16. Plot of $10 \log_{10} d_{\text{free}}^2$ versus complexity β for $R_{\text{eff}} = 1.0, 2.0,$ and 3.0 bit/T.

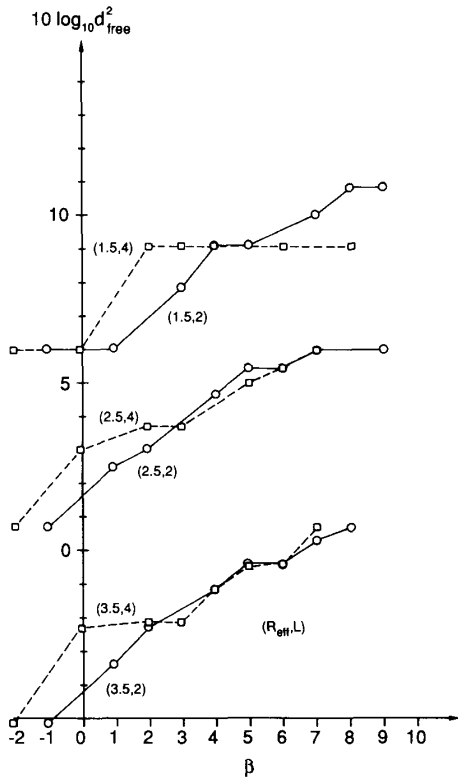


Fig. 17. Plot of $10 \log_{10} d_{\text{free}}^2$ versus complexity β for $R_{\text{eff}} = 1.5, 2.5,$ and 3.5 bit/T.

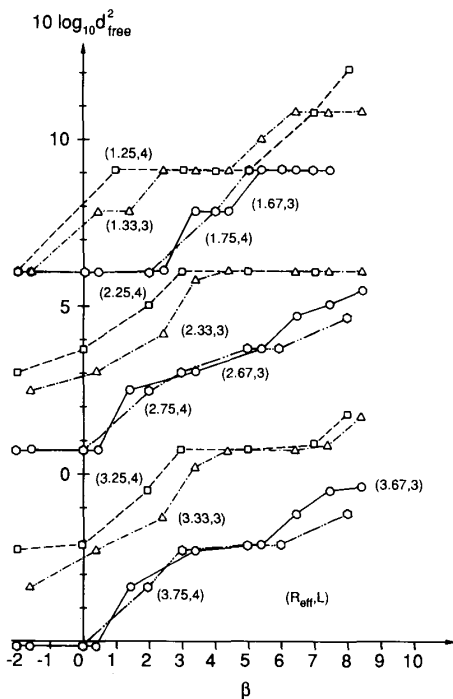


Fig. 18. Plot of $10 \log_{10} d_{\text{free}}^2$ versus complexity β for $R_{\text{eff}} = 1.25, 1.33, 1.67, 1.75, 2.25, 2.33, 2.67, 2.75, 3.25, 3.33, 3.67,$ and 3.75 bit/T.

Note from Fig. 16 for TC- $L \times 8$ PSK, $R_{\text{eff}} = 2.0$ bit/T, and $v=1$, that as L increases the complexity decreases and γ^* increases, eventually reaching 6.0 dB for $L=4$. Thus, for the 8D signal set, the complexity factor can be reduced by a factor of four, while maintaining γ^* , compared to the TC- 1×8 PSK code with $v=2$. Beyond $\beta=4$ (and $\gamma^* = 6.0$ dB), increases in asymptotic coding gain are achieved with the new codes that have been found. With $L=4$, a ceiling of $\gamma^* = 9.0$ dB will be reached due to the nature of the set partitioning. It would seem that very complex codes are required ($\beta \geq 15$) if this 9.0 dB limit is to be exceeded.

Fig. 16 also shows the $L \times 16$ PSK codes with effective rates of 3.0 bit/T. For small β , the same effect observed for TC- $L \times 8$ PSK and 2.0 bit/T occurs. That is, β decreases and γ^* increases as L increases. Between $\beta=3$ and $\beta=9$, the $L=1$ and $L=2$ codes are very close.

Fig. 18 illustrates the wide range of performance that can be achieved with the codes found. One can choose from a high-rate code with 3.75 bit/T (but requiring a large amount of power) to a low-rate code with 1.25 bit/T. In choosing a code, a designer may start with a required R_{eff} to obtain a certain bit rate through a bandwidth constrained channel. A trade-off can then be made between decoder complexity and the reduction in SNR that can be achieved with the codes found. Simulations or theoretical calculations of a few selected codes may also be made to obtain a more realistic assessment of the performance available.

Note that many codes have the same asymptotic coding gain for increasing complexity. In reality, these codes do increase in performance with increasing complexity due to a decrease in number of nearest neighbors. This is especially noticeable for low SNR where the effect of nearest neighbors becomes more important.

IV. CONCLUSION

An efficient method of partitioning multidimensional MPSK signal sets has been presented that leads to easily implemented multi-D signal set mappers. When these signal sets are combined with trellis codes to form a rate $k/(k+1)$ code, significant asymptotic coding gains in comparison to an uncoded system are achieved. These codes provide a number of advantages compared to trellis codes with 2-D signal sets. Most importantly, R_{eff} can vary from $I-1$ to $I-(1/L)$ bit/T, allowing the coding system designer a greater choice of data rates without sacrificing data quality. As R_{eff} approaches I , though, increased coding effort (in terms of decoder complexity) or higher SNR is required to achieve the same data performance.

The analytical description of multi-D signal sets in terms of block code cosets, and the use of systematic convolutional encoding, has resulted in an encoder design (from the differential encoder to the 2-D signal set mapper) that allows many good codes to be found. This approach has also led to the construction of signal sets

that allow codes to be transparent to multiples of $360^\circ/M$ phase rotations. In general, increasing phase transparency usually results in lower code performance, due to more nearest or next nearest neighbors or smaller free distance.

Another advantage is decoder complexity. As a Viterbi decoder decodes k bits in each recursion of the algorithm, the large values of k of codes using multi-D signal sets allows very high bit rates to be achieved (compared to convolutional codes that map only into a 2-D signal set). The large number of branch metric computations can be reduced either through the use of a modified Viterbi algorithm or large lookup tables. A method has been presented that uses the redundancy in some signal sets to achieve symbol synchronization at the decoder for codes that are not fully transparent.

Rate $k/(k+1)$ TC-L \times MPSK codes also have the advantage of being useful as inner codes in a high rate concatenated coding system with Reed-Solomon (RS) outer codes over $GF(2^k)$. If the inner decoder makes errors, one trellis branch error will exactly match one symbol in the outer RS codeword. It is shown in [14] that the symbol oriented nature of TC-L \times MPSK inner codes can provide an improvement of up to 1 dB in the overall performance of a concatenated coding system when these codes replace bit oriented TC-1 \times MPSK inner codes of the same rate.

APPENDIX DIFFERENTIAL ENCODING AND DECODING

Let the bit streams that are differentially encoded be $w^{c_0}(D), w^{c_1}(D), \dots, w^{c_{s-1}}(D)$. We first assume that $c_0 > 0$ (i.e., the convolutional encoder output $z^0(D)$ is not affected by a phase rotation of $2^d\Psi$, where $d = I - s$). Let

$$w(D) = \sum_{i=0}^{s-1} 2^i w^{c_i}(D). \quad (\text{A.1})$$

The differential encoder (or precoder) outputs are the bit streams $x^{c_0}(D), x^{c_1}(D), \dots, x^{c_{s-1}}(D)$ which go into the convolutional encoder. In a manner similar to (A.1), we let

$$x(D) = \sum_{i=0}^{s-1} 2^i x^{c_i}(D). \quad (\text{A.2})$$

For the noiseless channel we let the Viterbi decoder output which goes into the differential decoder (or postcoder) be $x_r(D)$ and the output from the postcoder be $w_r(D)$. After a $2^d\Psi$ phase rotation, we have from Section III-B that

$$x_r(D) = x(D) + 1(D) \pmod{S} \quad (\text{A.3})$$

where $S = 2^s$ and $1(D)$ is the all-ones sequence. For the postcoder, we desire that $w_r(D) = w(D)$ for all multiples of $2^d\Psi$ phase rotations. This is achieved by defining the postcoder equation as

$$w_r(D) = ((S-1)D+1)x_r(D) \pmod{S}. \quad (\text{A.4})$$

Substituting (A.3) into (A.4), we obtain

$$\begin{aligned} w_r(D) &= ((S-1)D+1)(x(D)+1(D)) \pmod{S} \\ &= ((S-1)D+1)x(D) \\ &\quad + ((S-1)D+1)1(D) \pmod{S} \\ &= w(D) + (S-1)1(D) + 1(D) \pmod{S} \\ &= w(D) + (S)1(D) \pmod{S} \\ &= w(D), \end{aligned}$$

as required. Notice that since $1(D)$ is defined to be 1 for all time, then $D^i 1(D) = 1(D)$ for all i . In practical situations, the sequence added to $x(D)$ to form $x_r(D)$ is not constant and will change with time (e.g., random phase slips within a demodulator). This will introduce short error bursts in $w_r(D)$ whenever a phase slip occurs due to the combined effect of decoding and postcoding. The precoder equation can be derived from (A.4) as

$$x(D) = Dx(D) + w(D) \pmod{S}. \quad (\text{A.5})$$

We shall now consider the case when $c_0 = 0$, i.e., $z^0(D)$ is affected by a $2^d\Psi$ phase rotation. In this case we redefine $w(D)$ to be

$$w(D) = \sum_{i=1}^{s-1} 2^{i-1} w^{c_i}(D) \quad (\text{A.6})$$

and $x(D)$ to be

$$x(D) = \sum_{i=1}^{s-1} 2^{i-1} x^{c_i}(D). \quad (\text{A.7})$$

For this case, we have $2x_r(D) + z_r^0(D) = 2x(D) + z^0(D) + 1(D)$, where $x_r(D)$ and $z_r^0(D)$ are the inputs to the postcoder for a noiseless channel. Thus similar to (A.4), the postcoder equation is defined to be

$$2w_r(D) = ((S-1)D+1)(2x_r(D) + z_r^0(D)) \pmod{S}. \quad (\text{A.8})$$

Rearranging (A.8), we obtain the precoder equation

$$2x(D) = 2Dx(D) + 2w(D) + (D+S-1)z^0(D) \pmod{S}. \quad (\text{A.9})$$

REFERENCES

- [1] G. Ungerboeck, "Channel coding with multilevel/phase signals," *IEEE Trans. Inform. Theory*, vol. IT-28, pp. 55-67, Jan. 1982.
- [2] G. D. Forney, Jr., R. G. Gallager, G. R. Lang, F. M. Longstaff, and S. U. Qureshi, "Efficient modulation for band-limited channels," *IEEE J. Sel. Areas Commun.*, vol. SAC-2, pp. 632-647, Sept. 1984.
- [3] A. R. Calderbank and J. E. Mazo, "A new description of trellis codes," *IEEE Trans. Inform. Theory*, vol. IT-30, pp. 784-791, Nov. 1984.
- [4] G. Ungerboeck, "Trellis-coded modulation with redundant signal sets: Parts I and II," *IEEE Commun. Mag.*, vol. 25, pp. 5-21, Feb. 1987.
- [5] D. P. Taylor and H. C. Chan, "A simulation study of two bandwidth efficient modulation techniques," *IEEE Trans. Commun.*, vol. COM-29, pp. 267-275, Mar. 1981.
- [6] S. G. Wilson, H. A. Sleeper, P. J. Schottler, and M. T. Lyons, "Rate 3/4 convolutional coding of 16PSK: code design and performance study," *IEEE Trans. Commun.*, vol. COM-32, pp. 1308-1315, Dec. 1984.
- [7] A. R. Calderbank and N. J. A. Sloane, "Four-dimensional modulation with an eight state trellis code," *AT&T Tech. J.*, vol. 64, no. 5, pp. 1005-1018, May-June 1985.
- [8] A. Lafanchère and D. J. Costello, Jr., "Multidimensional coded PSK systems using unit-memory trellis codes," in *Proc. Allerton*

- Conf. Commun., Cont., and Comput.*, Monticello, IL, Sept. 1985, pp. 428–429.
- [9] S. G. Wilson, "Rate 5/6 trellis-coded 8PSK," *IEEE Trans. Commun.*, vol. COM-34, pp. 1045–1049, Oct. 1986.
- [10] A. R. Calderbank and N. J. A. Sloane, "New trellis codes based on lattices and cosets," *IEEE Trans. Inform. Theory*, vol. IT-33, pp. 177–195, Mar. 1987.
- [11] L. F. Wei, "Trellis-coded modulation with multi-dimensional constellations," *IEEE Trans. Inform. Theory*, vol. IT-33, pp. 483–501, July 1987.
- [12] G. D. Forney, Jr., "Coset codes I: Introduction and geometrical classification," *IEEE Trans. Inform. Theory*, vol. 34, pp. 1123–1151, Sept. 1988, Part II.
- [13] ———, "Coset codes II: Binary lattices and related codes," *IEEE Trans. Inform. Theory*, vol. 34, pp. 1152–1187, Sept. 1988, Part II.
- [14] R. H. Deng and D. J. Costello, Jr., "High rate concatenated coding systems using multi-dimensional bandwidth efficient trellis inner codes," *IEEE Trans. Commun.*, vol. COM-37, pp. 1091–1096, Oct. 1989.
- [15] J. P. Odenwalder, "Optimal decoding of convolutional codes," Ph.D. dissertation, Univ. of California, Los Angeles, 1970.
- [16] H. Imai and S. Hirakawa, "A new multilevel coding method using error correcting codes," *IEEE Trans. Inform. Theory*, vol. IT-23, pp. 371–377, May 1977.
- [17] E. L. Cusack, "Error control codes for QAM signalling," *Electron. Lett.*, vol. 20, no. 2, pp. 62–63, 19 Jan. 1984.
- [18] V. V. Ginzburg, "Multidimensional signals for a continuous channel," *Problemy Peredachi Informatsii [Probl. Inform. Transmission]*, vol. 20, no. 1, pp. 28–46, Jan.–Mar. 1984 (in Russian).
- [19] S. I. Sayegh, "A class of optimum block codes in signal space," *IEEE Trans. Commun.*, vol. COM-34, pp. 1043–1045, Oct. 1986.
- [20] M. Rouanne and D. J. Costello, Jr., "A lower bound on the minimum Euclidean distance of trellis coded modulation schemes," *IEEE Trans. Inform. Theory*, vol. 34, pp. 1011–1020, Sept. 1988, Part I.
- [21] E. Zehavi and J. K. Wolf, "On the performance evaluation of trellis codes," *IEEE Trans. Inform. Theory*, vol. IT-33, pp. 196–202, Mar. 1987.
- [22] K. J. Larson, "Comments on 'An efficient algorithm for computing free distance,'" *IEEE Trans. Inform. Theory*, vol. IT-18, pp. 437–439, May 1972.
- [23] D. Divsalar and M. K. Simon, "Multiple trellis coded modulation (MTCM)," *IEEE Trans. Commun.*, vol. 36, pp. 410–419, Apr. 1988.
- [24] F. Hemmati and R. J. F. Fang, "Low complexity coding methods for high data rate channels," *Comsat Tech. Rev.*, vol. 16, pp. 425–447, Fall 1986.
- [25] S. S. Pietrobon, "Rotationally invariant convolutional codes for MPSK modulation and implementation of Viterbi decoders," masters thesis, South Australian Inst. of Technol., Adelaide, June 1988.
- [26] A. Michie and M. J. Miller, "Forward error correction using block coded multidimensional signals and soft decision decoding," in *Proc. IRECON '87*, Sydney, Australia, Sept. 1987, pp. 242–244.
- [27] E. Biglieri and M. Elia, "Multidimensional modulation and coding," *IEEE Trans. Inform. Theory*, vol. 34, pp. 803–809, July 1988.
- [28] A. R. Calderbank, "Multilevel codes and multistage decoding," *IEEE Trans. Commun.*, vol. 37, pp. 222–229, Mar. 1989.
- [29] G. J. Pottie and D. P. Taylor, "Multilevel codes based on partitioning," *IEEE Trans. Inform. Theory*, vol. 35, pp. 87–98, Jan. 1989.
- [30] F. P. Kschischang, P. G. de Buda, and S. Pasupathy, "Block coset codes for M -ary phase shift keying," *IEEE J. Sel. Areas Commun.*, vol. 7, pp. 900–913, Aug. 1989.
- [31] D. W. Lin, "Wide-band digital subscriber access with multidimensional block modulation and decision-feedback equalization," *IEEE J. Sel. Areas Commun.*, vol. 7, pp. 996–1005, Aug. 1989.
- [32] R. M. Tanner, "Algebraic construction of large Euclidean distance combined coding/modulation systems," *IEEE Trans. Inform. Theory*, to appear.
- [33] T. Kasami, T. Takata, T. Fujiwara, and S. Lin, "On multi-level block modulation codes," *IEEE Trans. Inform. Theory*, to appear.
- [34] ———, "On linear structure and phase rotation invariant properties of block 2^l -PSK modulation codes," *IEEE Trans. Inform. Theory*, to appear.